

LIQUID DISTRIBUTION FROM INDUSTRIAL SCALE SPRAY JETS IN
FLUIDIZED BEDS

(Spine Title: Liquid Distribution from Industrial Scale Spray Jets in Fluidized
Beds)

(Thesis Format: Integrated Article)

by

MohammadAli Zirgachianzadeh

Graduate Program
In
Engineering Science
Department of Chemical and Biochemical Engineering

A thesis submitted in partial fulfillment of the requirements for the degree of
Master of Engineering Science

The School of Graduate and Postdoctoral Studies
Western University
London, Ontario Canada

© MohammadAli Zirgachianzadeh 2012

Western University
School of Graduate and Postdoctoral Studies

Certificate of Examination

Joint-Supervisor

Dr. Cedric Briens

Joint-Supervisor

Dr. Franco Berruti

Examiners

Dr. Sohrab Rohani

Dr. Hui Zhang

Dr. Kamran Siddiqui

The thesis by

MohammadAli Zirgachianzadeh

entitled:

Liquid Distribution from Industrial Scale Spray Jets in Fluidized Beds

is accepted in partial fulfillment of the
requirements for the degree of
Master of Engineering Science

Date _____

Chair of the Thesis Examination Board

Abstract

Liquid injections via spray nozzles are used in fluidized bed reactors such as Fluid Cokers. In such industrial processes, in order to maximize the product yields it is required to optimize the performance of the nozzle. Moreover parts of the bed might become defluidized, bogged, due to a high liquid load. Then optimizing the performance of the nozzle and local bed bogging detection is the primary research objectives for this thesis work.

The first part of the research work was focused on developing a novel method employing electrical conductance to characterize the liquid distribution in a large scale fluid bed of about 7 tonnes of silica sand, using a commercial-scale spray nozzle. It was used to determine the effect of increasing atomization gas-to-liquid ratio on the liquid-solid contact efficiency. Electrodes have been employed to map the free moisture distribution through the entire bed. The results indicated that raising the G/L ratio improves the contact efficiency, especially at high G/L ratios.

Implementing the conductance method, the effect of a new device, consisting of a draft tube located downstream of the nozzle, on liquid distribution inside the large fluidized bed was studied next. It not only remarkably reduced the liquid trapped within wet agglomerates, but also greatly enhanced the distribution of injected liquid feed and the jet penetration of the nozzle.

Finally, the electrical conductance and several other experimental methods, such as differential and static pressure measurements, and image processing were successfully implemented to detect local bogging in the large scale pilot fluid bed.

Keywords:

Fluid Bed, Spray Nozzle, Liquid Injection, Fluid Coking, Measurement Technique, Electric Conductance, Draft Tube, Defluidization, Bogging, Fluidity

Co-Authorship

Chapter 2

Article Title: Electric conductance method for the assessment of liquid-gas injection into a large gas-solid fluidized bed
Authors: MohammadAli Zirgachianzadeh, Mehran Soleimani, Cedric Briens, Franco Berruti
Article Status: Unpublished
Contributions: MohammadAli Zirgachianzadeh conducted all experimental work, data analysis and writing. Mehran Soleimani assisted with setting up the fluidized bed, also assisted in some of the experimental work. Cedric Briens and Franco Berruti provided guidance, supervision and revised drafts of the work.

Chapter 3

Article Title: Impact of draft tube on industrial-scale Fluid Coker spray jets in fluidized beds
Authors: MohammadAli Zirgachianzadeh, Cedric Briens, Franco Berruti, Jennifer McMillan
Article Status: Unpublished
Contributions: MohammadAli Zirgachianzadeh conducted all experimental work, data analysis and writing. Cedric Briens, Franco Berruti and Jennifer McMillan provided guidance, supervision and revised drafts of the work.

Chapter 4

Article Title: In-situ characterization of bed fluidity in a large gas-solid fluidized bed via electric conductance method
Authors: MohammadAli Zirgachianzadeh, Cedric Briens, Franco Berruti, Jennifer McMillan
Article Status: Unpublished
Contributions: MohammadAli Zirgachianzadeh conducted all experimental work, data analysis and writing. Cedric Briens, Franco Berruti and Jennifer McMillan provided guidance, supervision and revised drafts of the work.

Acknowledgements

First and foremost, I am grateful to my supervisors Dr. Cedric Briens and Dr. Franco Berruti, from the Institute of Chemicals and Fuels from Alternative Resources (ICFAR) at the Western University, for their valuable guidance, mentorship, and advice. Their support throughout my studies was truly appreciated. I would like to thank Dr. Eb Mueller, Dr. Jennifer McMillan and Dr. Craig McKnight, of Syncrude Canada, for providing excellent feedback and support.

Deepest gratitude is also due to my post-doctoral fellow of ICFAR, Dr. Mehran Soleimani without whose knowledge and assistance this study would not have been successful. I would also like to thank Dr. Tarek J. Jamaledine, for providing me valuable advices and assistance on all my experimental works. Special thanks to Rob Taylor for his help on my experimental equipments. My appreciations also go to all my colleagues from ICFAR.

Finally, I am forever indebted to my parents, Mahmoud and Simin Borhani, and my beloved brother and sister for their understanding, endless patience and encouragement when it was most required.

Dedications

This thesis is dedicated to my father, who taught me that the best kind of knowledge to have is that which is learned for its own sake. It is also dedicated to my mother, who taught me that even the largest task can be accomplished if it is done one step at a time.

Table of Contents

Certificate of Examination	ii
Abstract	iii
Co-Authorship.....	v
Acknowledgements	vi
DEDICATIONS	vii
Table of Contents	viii
List of Figures	x
List of Tables	xii
Chapter 1: Introduction.....	1
1.1 Present Thesis Work.....	1
1.2 Fluid Coker.....	1
1.3 Review of conducted measurements in fluidized beds	4
1.3.1 Review of moisture measurement techniques in fluidized beds	4
1.3.2 Review of effect of nozzle operating conditions and draft tube on injection quality in fluidized beds	8
1.3.3 Review of bed fluidity measurement techniques in fluidized beds	9
1.4 Research Objectives	10
1.5 Nomenclature	12
1.6 References	12
Chapter 2: Electric conductance method for the assessment of liquid-gas injection into a large gas-solid fluidized bed	16
2.1 Introduction	16
2.2 Apparatus	19
2.3 Experimental Procedure	25
2.3.1 Experiments procedure	25
2.3.2 Calibration Experiments Procedure	26
2.4 Results	28
2.4.1 Variation of the bed conductance over the length of typical experiments..	28
2.4.2 Calibration experiments	30
2.4.3 Effect of GLR on injection quality	31
2.4.4 Effect of GLR on feed distribution across the bed.....	33
2.5 Conclusion.....	36
2.6 Nomenclature	36

2.7	References	37
Chapter 3: Impact of draft tube on industrial-scale Fluid Coker spray jets in fluidized beds 39		
3.1	Introduction	39
3.2	Apparatus	41
3.3	Experimental Procedure	44
3.3.1	Experiments procedure	44
3.3.2	Calibration Experiments Procedure	45
3.4	Results	46
3.4.1	Calibration.....	46
3.4.2	Comparison of ESE and Free Jet in terms of injection quality.....	47
3.4.3	Comparison in terms of feed distribution across the bed.....	49
3.5	Conclusion.....	54
3.6	Nomenclature	54
3.7	References	55
Chapter 4: In-situ characterization of bed fluidity in a large gas-solid fluidized bed via electric conductance method..... 57		
4.1	Introduction	57
4.2	Apparatus	60
4.3	Experimental Procedure	64
4.4	Results	66
4.4.1	Effect of Free Moisture on Bogging	66
4.4.2	Verification that Bogging Depends on Free Moisture	75
4.5	Conclusion.....	77
4.6	Nomenclature	77
4.7	References	78
Chapter 5: Conclusions and Recommendations		
5.1	Conclusions	81
5.2	Recommendations	82
Curriculum Vitae		83

List of Figures

Figure 1.1 Fluid coking process schematic diagram (adapted from House, 2007).....	4
Figure 2.1 Schematic diagram of the experimental set-up.....	20
Figure 2.2 Experimental apparatus picture	21
Figure 2.3 a Pie shaped slice cut out of the Fluid Coker cross section.....	21
Figure 2.4 Top view of the bed.....	22
Figure 2.5 TEB Nozzle Scheme.....	22
Figure 2.6 Schematic diagram of the electrodes configuration	23
Figure 2.7 Circuit diagram of conductance technique	24
Figure 2.8 Schematic diagram of electrodes circuit.....	24
Figure 2.9 Conductance signal variation with time after the injections of GLR=2.24%. All the injections started at 126 s.	28
Figure 2.10 Pre-mixer pressure during injection for various GLR percentages from 0 to 3.5%, mliq=1.47 kg/s	29
Figure 2.11 Left: Calibration curve of Electrode9, Right: Calibration curve of Electrode 10.....	30
Figure 2.12 Coordinates of the electrodes in the bed.....	31
Figure 2.13 Effect of GLR on injection quality taking into account the width of the bed	33
Figure 2.14 Image of the bed for different GLR's (a to i); Z axis: Local τ	35
Figure 3.1 Schematic diagram of the experimental set-up.....	42
Figure 3.2 Experimental apparatus picture	42
Figure 3.3 Top view of the bed.....	42
Figure 3.4 TEB Nozzle Scheme.....	43
Figure 3.5 Nozzle Assembly Scheme (ESE)	43
Figure 3.6 Left: Calibration curve of Electrode9, Right: Calibration curve of Electrode 10	46
Figure 3.7 Effect of GLR on injection quality with ESE nozzle	47
Figure 3.8 Coordinates of the electrodes in the bed.....	48
Figure 3.9 Effect of GLR on injection quality taking into account the width of the bed for ESE nozzle	49
Figure 3.10 Comparison of images of the bed for ESE and TEB nozzles for different GLR's (a to r).....	53
Figure 3.11 Comparison of two different GLR's of ESE and TEB which have similar injection quality	53
Figure 4.1 Schematic diagram of the experimental set-up.....	61
Figure 4.2 Experimental apparatus picture	62
Figure 4.3 Top view of the bed.....	62
Figure 4.4 TEB Nozzle Scheme.....	62
Figure 4.5 Camera set up in front of the window	63
Figure 4.6 Schematic diagram of sensors configuration.....	64
Figure 4.7 Wind box configuration.....	65
Figure 4.8 Calibration Curve for the defluidized bed	66
Figure 4.9 Left: bubbles going through the bed, Right: air being stuck in the sands	67
Figure 4.10 Image Processing results	67

Figure 4.11 Conductance signal variation with time after the injections of GLR=2.24%. All the injections started at 126 s. Electrode 12.....	68
Figure 4.12 Electrode 12 th signal when there is no local bogging	69
Figure 4.13 Electrode 12th signal with local bogging	70
Figure 4.14 Electrode 11th signal when its facing area has been bogged for a while	70
Figure 4.15 Coefficient of Variance of the twelfth electrode	71
Figure 4.16 Differential Pressure Transducer signal when low liquid load is injected (L/S = 0.024%), non-bogged conditions	72
Figure 4.17 Differential Pressure Transducer signal when high liquid load is injected (L/S = 0.047%), bogged conditions	72
Figure 4.18 Coefficient of variance of the Differential Pressure Transducer signal	73
Figure 4.19 Coefficient of variance of the Flush Diagram Pressure Transducer signal ...	74
Figure 4.20 Absolute difference between thermocouples signals in bogging and non- bogging zones	75
Figure 4.21 Coefficient of variance of electrode 12 for different GLR's	76
Figure 4.22 Coefficient of variance of the Differential Pressure Transducer for different GLR's.....	76
Figure 4.23 Coefficient of variance of the Flush Diagram Pressure Transducer for different GLR's	77

List of Tables

Table 1-1 Extra-heavy oil and oil sands resources (billion barrels)	2
Table 2-1 Remarkable agreement between the bed solid moisture found from sampling and the real one	28
Table 2-2 Accordance between injected water and calculated evaporated water.....	31
Table 3-1 Remarkable agreement between the bed solid moisture found from sampling and the real one	46
Table 3-2 Accordance between injected water and calculated evaporated water.....	47

Chapter 1: Introduction

1.1 Present Thesis Work

The research presented in this dissertation addresses the interaction between a gas-liquid jet and a gas-solid large scale fluidized bed similar to that of used in Fluid Coking processes for upgrading heavy oil. A novel method using electrical conductance has been applied for the purpose of mapping the liquid-solid contact quality across the entire bed. The main objective of the thesis is to improve the efficiency of the liquid-solid contact and also the bed fluidity in Fluid Coking processes by changing the atomization gas flowrate through an industrial size feed nozzle, same as the one used in a Fluid Coker, as well as the configuration of the spray nozzle assembly.

In this chapter, experimental studies of methods implemented to assess the jet bed interaction are discussed. A brief explanation of the fluid coking process follows; provided that the key motivational factor for this thesis is to improve the fluid coking process. The remainder of this chapter then introduces some of the key recent studies on the methods used for addressing the liquid-solid contact quality, the effect of nozzle associated parameters on this quality, and the suitable techniques for industrial detection of localized bed defluidization in a fluid bed. And finally, an overview of the research objectives for this work is stated.

1.2 Fluid Coker

Heavy oils are characterized by low hydrogen to carbon ratios and high carbon residues, asphaltenes, nitrogen, sulfur, metal contents, and generally an API lower than 20; it would be 10 for extra heavy oils and bitumens.

Currently the volume in light oils is declining and feedstocks are getting heavier. Oil companies are exploring new and more challenging locations with regard to the significant quantities of heavy oil throughout the world, most of which have not been developed due to the logistical challenges and cost of production using conventional technologies.

	Extra-heavy oil			Oil sands		
	Oil in place	Recovery factor	Technically recoverable	Oil in place	Recovery factor	Technically recoverable
World resources	404	0.40	158	4150	0.33	1370

Table 1-1 Extra-heavy oil and oil sands resources (billion barrels)

Table 1-1 Extra-heavy oil and oil sands resources (billion barrels) shows the extra-heavy oil and oil sands resources in the world [1, 2]; recovery factor can be changed depending on the economic situation and technology improvement. These numbers highlight the importance of the unconventional oils in the future energy scenario and for these reasons the International Energy Agency (IEA) foresees a growing role for both heavy oil and bitumen in the medium-long term [2].

The greater part of these reserves is concentrated in Canada, in the province of Alberta (tar sands), and in Venezuela in the so called Orinoco Belt. A third country which is rich in non-conventional oil is Russia, even though in this case the deposits are scattered so that the recoverable portions are not quantitatively as large as in the other two countries [3].

There are a variety of processes designed to upgrade these heavy oil feedstock to more valuable products. The main scope of a conversion/upgrading technologies is to:

- Convert the atmospheric & vacuum residues into distillates minimizing the by-products
- Remove poisons such as heteroatoms (i.e. sulphur, nitrogen and oxygen), asphaltenes and metals
- Increase the hydrogen content of the upgraded materials [4].

The increase of the H/C ratio can be made either rejecting carbon or adding hydrogen. The C-rejection processes (such as coking and fluid coking) show very high feedstock flexibility but generate low quality distillates and huge amount of by-products, such as pet-coke and fuel oil—the latter market demand is shrinking [5]. That is why companies running fluid cokers for upgrading the heavy oil, such as Syncrude Canada

Ltd., have decided to investigate ways improving the efficiency of fluid coking operations. Syncrude Canada Ltd. is one of the largest manufacturers of crude oil from Canada's oil sands, with the three largest Fluid Cokers in the world. Syncrude Canada Ltd. produced 107 million barrels of crude oil from oil sands bitumen in 2010 and is capable of supplying 15% of Canada's petroleum requirements (Syncrude Canada Ltd., 2011).

Figure 1.1 Fluid coking process schematic diagram (adapted from House, 2007) provides a flow diagram of the Fluid Coking process. A commercial Fluid Coking reactor has an average diameter of approximately 9.8 m and a bed height to diameter ratio of 2.18 [6]. Syncrude Fluid Coking system is composed of two vessels which are operated simultaneously: the fluid bed reactor and the fluid bed burner (or regenerator). The liquid bitumen feed is atomized with steam and then injected at 350 °C into a fluidized bed reactor of coke particles at 510-550 °C through 70-80 horizontally oriented injection nozzles. The configuration is like a ring of nozzles that encircles the circumference of the reactor, spaced vertically along the reactor. These hot coke particles provide the heat required to initiate the endothermic cracking reactions occurring in the feed droplets as the liquid deposits on the surface of coke particles. The products of the cracking reactions are a mixture of gases, light and heavy gas oils, and coke. The cracked vapors rise up the reactor, and as more feed is injected, the gas flow rate increases with height in the reactor. To moderate the increase in gas velocity, the reactor has conical section [7]. The cracked vapours rise up the reactor and cyclones located at the top of the vessel remove entrained coke particles and return them to the dense bed of the reactor. The condensable vapour products pass through a scrubber and are then further processed downstream. A fraction of feed devolatilizes before undergoing significant cracking is recycled to the feed nozzles. Coke particles are circulated to a burner where they are heated to about 630 °C and a fraction of this coke is recycled to provide heat for the reactor. The remaining coke is waste which must be stored or discarded [8]. The light and heavy gas oils which can be mixed to form synthetic crude oil are the most valuable products. Therefore, the aim of Fluid Coking is to maximize the production of these products while minimizing the formation of lighter gases and coke [9].

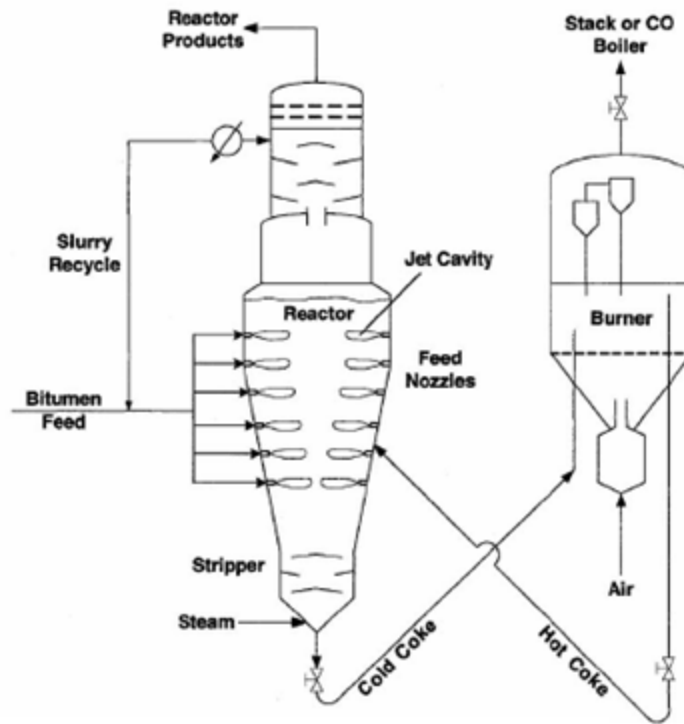


Figure 1.1 Fluid coking process schematic diagram (adapted from House, 2007)

1.3 Review of conducted measurements in fluidized beds

This section outlines different studies that have investigated various aspects associated with gas-liquid injections using several measurement techniques. Emphasis is placed on slow-evaporating liquid injections, such as the ones used in the Fluid Coking process.

1.3.1 Review of moisture measurement techniques in fluidized beds

Although several measuring techniques are available for assessing the moisture content of solid materials, especially in soils, such as Time domain reflectometry, neutron absorption, near-infrared reflectance (NIR), and microwave spectrometry [10-18], few were aimed at assessing the quality of the jet-bed interaction, i.e. the contact between injected liquid and fluidized particles, and those that did have not been tested for large scale fluid bed plant applications.

A technique was developed by McMillan et al. [19, 20] to assess the local quality of the liquid–solid mixing within the liquid jet cavity by measuring the local bed temperature at numerous locations in the jet region. While this method can be easily scaled up, it only measures the liquid–solid contact within the jet cavity.

In another study, steam-atomized bitumen was injected by Knapper et al. [21] into a scaled down fluid coker. Copper naphthenate was added as a tracer to the injection. The coke particles would be coated with copper deposits where the bitumen reacted. Energy-dispersive X-ray was applied to measure the copper concentration in the coke samples taken from the pilot plant coker. In order to find the copper content of the coke particles, inductively couple plasma (ICP) was also used. Although the fluidization velocity, 0.3 m/s, was high enough for a decent mixing, only a small fraction of coke particles were coated with the copper trace meaning the liquid-solid contact efficiency in fluid coker is very low. Given the good mixing quality, it also emphasizes the need for a better injection. The technique used in this study was beneficial as it can be used under the operating conditions used in an industrial unit; however, it is a complicated process, is quite time consuming, and the tracer contaminates the coke particles used in the coker.

Eventually a new rapid and reliable experimental technique using electrical conductance was implemented by Leach et al. [22] to evaluate the liquid-solid contact efficiency in a fluidized bed. They used a rectangular air-fluidized bed of silica sand particles with dimensions of 1 m x 0.3 m, and a height of 3.2 m. An electrode probe, i.e. a hollow tube, was placed on the opposite side of the bed with respect to the injection nozzle, above the gas distributor and below the nozzle height extending 0.65 m into the bed. A nylon fitting was applied to insulate the probe from the grounded metal walls of the fluidized bed. The electric current flowing from the probe to the ground was converted to a voltage, amplified and recorded by a data acquisition. The bed was defluidized after the injection, in order to prevent the breakup of wetter and bigger agglomerates, and then the conductance signal was measured. Dry solid particles acquire electrostatic charges by friction on the bed walls, other random particles and various internals during fluidization. The triboelectric charges accumulated on the fluidized particles that come in contact with an electrode will discharge to the ground if the

grounded electrode is inserted into the bed. When the bed is defluidized, this generation of triboelectric charges is stopped, and the charges produced during fluidization will gradually discharge to the ground. The discharge is very slowly in a dry defluidized bed of low-conductivity particles, such as silica sand particles, with respect to the wetted defluidized bed solids with water. In addition, if the water is well distributed throughout the particles, there will be a larger number of high conductivity paths, resulting in a higher rate of electrical discharge. Therefore, the intensity of the current flowing through the electrode was used to assess the nozzle performance as well as the effect of increasing the gas-to-liquid mass ratio (G/L) through the nozzle on the liquid–solid contact efficiency. This new method gave results that agreed well with the results obtained with previous techniques of measuring the triboelectric current during fluidization, but was more convenient and more reproducible. The results show that small changes to the atomization nozzle geometry can greatly improve liquid-solid contact in the bed, especially at relatively high gas to liquid ratios in the injection nozzle. A mathematical model was also established to correlate the electric current to the quality of the liquid distribution.

Portoghese et al. [23] then refined this technique by applying a sinusoidal current to the fluidized bed and measuring the voltage drop across the fluidized bed, in order to find its conductance. They also positioned the electrical probe below the nozzle, and above the grounded distributor, rather than putting it in the opposite side of the nozzle. The dimension of the rectangular fluid bed was 1.2 m x 0.15 m with a height of 2.8 m and silica sand particles were used. An AC voltage was applied between a measurement resistor connected in series with the electrode, and the ground. For a given applied voltage, and a given measurement resistance, electric behavior of the bed material interposed between the electrode and the grounded bed walls affect both the amplitude and the phase of the alternating current.

Right after the end of the liquid injection the fluidization air was stopped and conductance was measured when the bed solids were defluidized. The extent by which the bed electric conductance increased depended on the quality of the liquid-solid mixing achieved during the injection, prior to defluidizing the bed, a more uniform distribution of

the liquid over the particles resulting in a higher bed conductance. It was found that increasing GLR is beneficial for liquid-solid contact efficiency over the tested range of GLR (0–3.3 wt %). It was also expressed that the electric conductance method was both highly sensitive to changes in the nozzle operating conditions and reproducible. That's why they suggested implementing this method in larger fluidized beds which is basically what has been done in this thesis.

Subsequently Leach et al. [24] applied this method to evaluate and compare the liquid–solid contact performance of various commercial nozzles, as well as other custom-made nozzle designs, under a variety of operating conditions. They used the exact same electrical configuration as the one used by Portoghese et al. [23], but the same fluid bed as the one they had implemented in the study just mentioned, Leach et al. [22]. In addition, to measure the droplet size distribution in the nozzle jets some open-air tests were conducted. In this study also, the conductance method was successfully applied to characterize the performance of atomizing feed nozzles in their potential for injecting and distributing liquid into gas–solid fluidized beds. All of the nozzles showed a relationship between the gas-to-liquid ratio (GLR) and the quality of the liquid mixing; some types of the nozzles had an optimal gas-to-liquid ratio. Thus it is important to identify the optimum GLR for each nozzle and each liquid flow rate, which is what is also found in the chapter 1 of this dissertation.

In addition, it was found that when the size of the droplets was significantly larger than the size of the particles, the droplet size had a negative effect on the quality of the liquid–solid contact. When more gas was applied droplet sizes tended to decrease, but the relationship between droplet size and jet-bed interaction was different for each nozzle, confirming that nozzle geometry also has a significant effect. Thus, as it is concluded in Leach et al. work [25], when choosing parameters for an injection into a fluidized bed, special care should be taken in choosing the proper nozzle, as its geometry is the most critical parameter affecting the contact between sprayed liquid and fluidized particles.

Thus, following the suggestion of the authors of the previously developed conductance method [22, 23, 24] in small scales for implementing this technique in large scale fluid beds, the objective of this study was to apply this method in a large scale fluid

bed. But a new configuration had to be applied in order to be able to see the moisture distribution all over the bed.

1.3.2 Review of effect of nozzle operating conditions and draft tube on injection quality in fluidized beds

Several methods have been implemented to study the effect of the amount of atomization gas and a draft tube on the liquid and solid particles contact. For example, the initial liquid–solid mixing was assessed by House et al. [26] via injecting a binder solution into a fluid bed of coke particles. The binding agent was made by adding sucrose to the injected liquid (21 wt% sucrose). Shortly after the liquid injection fluidization gas was stopped in order to avoid breaking the agglomerates by mixing. By this way, agglomerates were preserved to see the effect of injection inclusively on them. Afterwards the stationary bed was aerated for approximately three hours. Then gravimetric analysis and enzymatic test were applied to find the liquid to solid mass ratios (L/S) of the agglomerates from the samples taken from the bed during the defluidization time. It was found that 50% of the wetted solids were agglomerates with a liquid to solid mass ratio between 0.05 to 0.15 wt% when the gas to liquid mass ratio in the injection was about 3 wt%. Then they added a draft tube to the injection nozzle assembly to see the effect; similar to the draft tube applied by McMillan and Hulet et al [20, 27], and the 2nd chapter of this thesis. This resulted in weaker agglomerates which had a L/S ration of under 0.08% and consequently could break more easily. Another conclusion of this study was that most of the liquid-solid contact took place at the tip of the jet cavity introduced by the injection nozzle. This study was important, as it presented a quantitative measurement of the liquid distribution in a fluidized bed, after an injection. However, the process is very time consuming, and could only be used on very small fluidized beds, as the sand becomes contaminated with sucrose and requires replacement.

On the other hand, larger triboelectric probes were used by Portoghese et al. [10, 11, 28, 29] to monitor the quality of liquid distribution in the wetted surface of a fluid bed. Silica sand particles were fluidized with air in the bed to which atomized water with air was injected. The positive effect of increasing the water flow rate and reducing the nozzle throat diameter was discovered. The pressure drop is increased when the throat diameter is decreased and consequently the droplets would become smaller. But this

method is sensitive to the bed hydrodynamics as it based on measuring the current produced by collisions inside the bed. On the other hand, the conductance method is much less sensitive to the local bed hydrodynamics [22, 23].

Small triboelectric pins, placed in a draft tube downstream of the nozzle, were implemented by Hulet et al. [27] to investigate the effect of different draft tube shapes on the solids entrainment and jet stability. An optimum distance between the spray nozzle and draft tube was found. It was also showed that the inlet configuration of the draft tube affects the entrainment level. Fortunately, the triboelectric probes were sensitive enough to the local disturbances in the liquid quantity, but caused remarkable amount of noise, and needed external electrical amplification and substantial signal analysis.

None of the above studies were performed with spray nozzles of a realistic size. Another objective of the present paper is, therefore, to evaluate the effect of the atomization gas flow rates and enhanced solids entrainment (ESE) device on the distribution of liquid sprayed into a fluidized bed with a commercial size nozzle.

1.3.3 Review of bed fluidity measurement techniques in fluidized beds

Various methods have been applied in the literature to detect the quality of fluidization. For instance, Bruhns et al. [30] applied a combination of capacitance probes, gas suction probes, and thermocouples to study the effect of liquid jet on the bed. Thermocouples were located at various axial and radial positions close to the nozzle tip. The characterization of both the penetration depth and expansion angle of the liquid spray was conducted by these local thermocouples. On the other hand, the changes in bed hydrodynamics was measured by the capacitance probe and the results were confirmed by gas suction probes which measured the vapor concentration. It was found that the gross solids mixing of the fluid bed rapidly transported the agglomerates into the interior. The liquid evaporates from the interior of the agglomerates and the effect of the vigorous particle–particle interactions in the fluid bed causes the agglomerates disintegration.

A technique was developed by Tsujimoto et al. [31], who employed an acoustic emission sensor in a fluidized bed granulator to detect unstable fluidization conditions, such as channelling and blocking, resulting from an excessive increase in solid moisture

content. It was found that the propagation of the acoustic waves is attenuated by the presence of moisture in the bed solids. Significant changes in the mean acoustic emission amplitude, however, would require moisture levels higher than 15%, which precludes the use of this technique for adequate measurements of solid moisture during fluid bed drying. Book et al. [32] investigated passive acoustic and vibrometric methods just recently and proved that they can be used for the detection and monitoring of the changes of bed fluidity in a large scale fluid bed caused by much smaller moisture levels. Also, Chaplin et al. [33] recently showed how the S-statistic analysis could be applied to pressure fluctuation data measured in a fluid bed dryer to monitor the bed hydrodynamics during drying of pharmaceutical granules. This technique provides an early detection of the onset of entrainment taking place when the granule moisture content is about 11 wt. %, but not the means to monitor the evolution of the bed moisture content during drying.

As these techniques have not been used in large scale, another objective of the study presented in this paper was to apply the bed conductivity method and other various lab techniques that are suitable for industrial reactors to detect the localized bed bogging in a large fluidized bed.

1.4 Research Objectives

The motivation for the present work is derived from the Syncrude fluid coking process. Syncrude is conducting research for the sake of improving the feed injection and subsequently the efficiency of its fluid cokers in order to be able to compete with its competitors, e.g. hydrocrackers, and also because of high worldwide demand of oil, huge quantity of the reserves in Canada's oil sands as well as high market prices.

Currently, the coker operating conditions have been gradually shifting towards higher throughput and heavier feed stocks. Recent developments to the coking process have sought to enhance the yield of valuable liquid products by lowering the coker operating temperature by 10-30 °C. In other words, high operating temperatures cause increased vapor phase cracking of valuable light and heavy gas-oils to the less valuable lighter gases. Reducing the coker temperature also lowers the amount of carbon rejected. This minimizes the amount of coke that needs to be burnt in the regenerator and, thus

lowers the sulfur dioxide emissions, contributing towards an eco-friendly and a more energy efficient process [7].

On the other hand, when the steam-bitumen mixture exits a feed nozzle, it expands to form a jet cavity in the fluidized bed. Particles from the fluidized bed are entrained into the jet cavity due to turbulent eddies formed at the jet-bed interface and due to suction created just downstream of the nozzle tip. Most of the initial contact between bed particles and atomized bitumen occurs in the jet or at the jet boundary, near its tip [9]. If the liquid-solid contact established in this region is poor, or in other words the distribution is poor, a thick liquid film will form and impose high heat and mass transfer limitations and lead to formation of agglomerates, and increased production of waster coke [26].

This poor distribution, moreover, limits the rate of cracking and product vaporization. Consequently, as mentioned before, given the bed temperatures could not be kept high enough to compensate for this poor contact, liquid may survive long enough that a significant fraction of liquid may enter the stripper. This section of the reactor contains solid internals called sheds which are designed to improve steam distribution for stripping excess hydrocarbons. However, liquid entering this region can cause severe fouling of these sheds. Stripper fouling causes shutdowns and constrains the operating conditions of commercial reactors [9].

Accordingly, the best solution to avoid agglomeration, to have better products, and to limit the rate of stripper fouling while having more valuable products and less waste coke in a fluid coker is to improve liquid-solid contact occurring in the jet cavity and at the jet bed boundary. If this better feed distribution is achieved, lower reactor temperatures can be used and less unwanted cracking of valuable light and heavy gas oils will occur in the vapor phase; however the effect of this on the bogging occurrence inside the bed should be also examined [9].

Lasheras et al. [34] found that, the Sauter mean diameter of the droplets produced at the centerline of a round water jet atomized by a jet decreased when the amount of atomization gas, or Gas to Liquid ratio (GLR) was increased. Sauter mean diameter is

defined as the diameter of a sphere that has the same volume/surface area ratio as a particle of interest. However, another study conducted by Portoghese et al. [28], showed that depending on nozzle size and operating liquid flow rate, an optimum GLR could be identified beyond which any further increase in GLR had negligible effect on nozzle performance. Moreover, McMillan et al. [20] showed that positioning a draft tube in front of the nozzle can also improve the efficiency of feed distribution in a fluid bed. In addition, in another study McDougall et al. [35] proved that increasing the liquid load will promote the possibility of defluidization in a fluid bed.

Therefore, the objective of the first study was to see the effect of changing GLR ratio in an industrial scale nozzle on the injection quality as well as feed distribution in a large fluid bed.

The objective of the second study was investigating the effect of installing a draft tube downstream of the nozzle used in the first study.

The objective of the third study was to examine the effect of changing the load of the liquid feed as well as GLR ratio, or free moisture, on the local bogging potential of the bed.

Thus in overall, the general objective of this thesis, which stems from Syncrude research focus, is to implement a new method using electrical conductance in a large scale gas-solid fluidized bed to address the effect of injection parameters on solid-liquid contact efficiency as well as bed fluidity.

1.5 Nomenclature

GLR Gas to Liquid Ratio

NIR Near-Infrared Reflectance

1.6 References

(1) Eni Corporation website

- (2) "World Energy Outlook 2004" provided by International Energy Agency
- (3) World Energy Council Report
- (4) Fujita, K.; Abe, S.; Inoue, Y.; Plantenga, P.L. and Leliveld, B. New Development in Residue Hydroprocessing, *Petroleum Tech. Quarterly*, Winter 2001-02, 51
- (5) Ellis, J. Paul, Tutorial: Delayed Coking Fundamentals, AIChE 1998 Spring National Meeting, New Orleans
- (6) Song, X.; Bi, H.; Lim, J.L.; Grace, J.R.; Chan, E.; Knapper, B.; McKnight, C. Hydrodynamics of the reactor section in fluid cokers. *Powder Technology*, 2004,147,126-136.
- (7) Ariyapadi, S. Interaction between Horizontal Gas-Liquid Jets and Gas-Solid Fluidized Beds. Thesis, The University of Western Ontario, London, Canada, **2004**.
- (8) Gray, M. Upgrading of petroleum residues and heavy oils; M. Dekker: New York,1994.
- (9) House, P. Interaction of Gas-Liquid Jets with Gas-Solid Fluidized Beds: Effect on Liquid-Solid Contact and Impact on Fluid Coker Operation. Thesis, The University of Western Ontario, London, Canada, **2007**.
- (10) Portoghese, F.; Berruti, F.; Briens, C. Use of triboelectric probes for on-line monitoring of liquid concentration in wet gas–solid fluidized beds. *Chemical Engineering Science* **2005**, 60, 6043-6048.
- (11) Portoghese, F.; Berruti, F.; Briens, C. Continuous on-line measurement of solid moisture content during fluidized bed drying using triboelectric probes. *Powder Technol* **2008**, 181, 169-177.
- (12) Watano, S.; Sato, Y.; Miyanami, K. Application of fuzzy logic to moisture control in fluidized bed granulation, *Journal of Chemical Engineering of Japan* 28 (3) **1995** 282–287.
- (13) Gawande, N.A.; Reinhart, D.R.; Thomas, P.A.; McCreanor, P.T.; Townsend, T.G. Municipal solid waste in situ moisture content measurement using an electrical resistance sensor, *Waste Management* 23 **2003** 667–674.
- (14) Evett, S.R. Soil water measurement by time domain reflectometry, *Encyclopedia of Water Science* **2003** 894–898.
- (15) Starr, J.L.; Paltineanu, I.C. Soil water measurement by capacitance, *Encyclopedia of Water Science* **2003** 885–888.
- (16) Evett, S.R. Soil water measurement by neutron thermalization, *Encyclopedia of Water Science* **2003** 889–893.
- (17) Webster, J.G. The measurement, instrumentation and sensors handbook. Editor-in-Chief J.G. Webster, CRC Press in cooperation with IEEE Press, 1999 72 pp. 11.
- (18) Watano, S.; Takashima, H.; Miyanami, K. Control of moisture content in fluidized bed granulation by neural network, *Journal of Chemical Engineering of Japan* 30 (2) **1997** 223–229.

- (19) McMillan, J.; Zhou, D.; Ariyapadi, S.; Briens, C.; Berruti, F.; Chan, E. Characterization of the contact between liquid spray droplets and particles in a fluidized bed, *Ind. Eng. Chem. Res.* 44 **2005** 4931– 4939.
- (20) McMillan, J.; Zhou, D.; Ariyapadi, S.; Briens, C.; Berruti, F.; Chan, E. Characterization of the contact between liquid spray droplets and particles in a fluidized bed, *Ind. Eng. Chem. Res.* 44 **2005** 4931– 4939.
- (21) Knapper, B.; Gray, M.; Chan, E.; Mikula, R. Measurement of efficiency of distribution of liquid feed in a gas–solid fluidized bed reactor, *Int. J. Chem. Reactor Eng.* 1 **2003**.
- (22) Leach, A.; Portoghese, F.; Briens, C.; Berruti, F. A new and rapid method for the evaluation of the liquid–solid contact resulting from liquid injection into a fluidized bed. *Powder Technol* **2008**, 184, 44-51.
- (23) Portoghese, F.; House, P.; Berruti, F.; Briens, C.; Adamiak, K.; Chan, E. Electric conductance method to study the contact of injected liquid with fluidized particles. *AICHE J.* **2008**, 54, 1770-1781.
- (24) Leach, A.; Chaplin, G.; Briens, C.; Berruti, F. Comparison of the performance of liquid–gas injection nozzles in a gas–solid fluidized bed. *Chemical Engineering and Processing: Process Intensification* **2009**, 48, 780-788.
- (25) Leach, A. Development of effective gas-atomized liquid injectors for fluidized beds. Thesis, The University of Western Ontario, London, Canada, **2009**.
- (26) House, P. K.; Saberian, M.; Briens, C. L.; Berruti, F.; Chan, E. Injection of a Liquid Spray into a Fluidized Bed: Particle–Liquid Mixing and Impact on Fluid Coker Yields. *Ind Eng Chem Res* **2004**, 43, 5663-5669.
- (27) Hulet, C.; Briens, C.; Berruti, F.; Chan, E.; Ariyapadi, S. Entrainment and Stability of a Horizontal Gas-Liquid jet in a Fluidized Bed. *Int. J. Chem. React. Eng.* **2003**, 1 (A60), 1127.
- (28) Portoghese, F.; Ferrante, L.; Berruti, F.; Briens, C.; Chan, E. Effect of injection-nozzle operating parameters on the interaction between a gas–liquid jet and a gas–solid fluidized bed. *Powder Technol* **2008**, 184, 1-10.
- (29) Portoghese, F.; Berruti, F.; Briens, C.; Chan, E. Novel triboelectric method for characterizing the performance of nozzles injecting gas-atomized liquid into a fluidized bed. *Chemical Engineering & Processing: Process Intensification* **2007**, 46, 924-934.
- (30) Bruhns S.; Werther J.; An investigation of the mechanism of liquid injection into fluidized beds, *AICHe J.* 51 **2005** 766–775.
- (31) Tsujimoto, H. ; Yokoyama, T.; Huang, C.C.; Sekiguchi, I. Monitoring particle fluidization in a fluidized bed granulator with an acoustic emission sensor, *Powder Technology* 113 **2000** 88–96.
- (32) Book, G.; Albion, K.; Briens, L.; Briens, C.; Berruti, F. On-line detection of bed fluidity in gas–solid fluidized beds with liquid injection by passive acoustic and vibrometric methods. *Powder Technol* **2011**, 205, 126-136.

- (33) Chaplin, G. ; Pugsley, T.; Winters, C. The S-statistic as an early warning of entrainment in a fluidized bed dryer containing pharmaceutical granule, Powder Technology 149 **2005** 148 156.
- (34) Lasheras J.C.; Villermaux E.; Hopfinger E.J.; Break-up and atomization of a round jet by a high-speed annular air jet, J. Fluid Mech. 357 **1998** 351–379.
- (35) McDougall, S.; Saberian, M.; Briens, C.; Berruti, F.; Chan, E. Characterization of fluidization quality in fluidized beds of wet particles, submitted to the IJCRE, **2004**.

Chapter 2: Electric conductance method for the assessment of liquid-gas injection into a large gas-solid fluidized bed

2.1 Introduction

A large number of chemical and petrochemical processes such as fluid coking, fluid catalytic cracking (FCC) and gas-phase polymerization utilize liquid-injections into a gas-solid fluidized bed. In industrial Fluid Cokers, bitumen is mixed with atomization steam prior to being injected into the reactor and then injected into a bed of solid coke particles, fluidized by steam and pre-heated to a temperature of about 550° C [1]. The fluidization of hot solid particles and atomizing the liquid with steam improves the liquid distribution leading to more rapid thermal cracking of the large hydrocarbon molecules in bitumen. Both the hydrocarbon conversion efficiency and the operability of the reactor are strongly affected by the initial contact between the injected liquid and the fluidized solids [2, 3, 4]. It has been shown that improving the contact of injected liquid with fluidized particles increases the yield of valuable liquid products in both the fluid catalytic cracking process, where most of the liquid is vaporizable, and in the fluid coking process, where most of the liquid is not directly vaporizable, but must first be cracked to generate vaporizable fractions [2, 3, 5]. When the liquid droplets injected into the bed from the nozzle are smaller, the contact between liquid-solids would be more uniform and accordingly better as the individual solid particles are more uniformly coated with the liquid particles; that is called a better injection quality of the nozzle.

In the case of vaporizable liquids, liquid-solid agglomerates may or may not be formed, depending on the operating conditions [6, 7], while they always form with non-vaporizable liquids [8]. If the fluidized bed mixing is not intense enough to ensure their rapid disintegration, the agglomerates are likely to survive for a relatively long time causing a significant portion of the injected liquid feed to be trapped within the agglomerates, and resulting in poor mass and heat transfer, which adversely affect the yields of valuable products and slows the cracking reactions [9, 3, 10].

Several methods have been implemented to study the effect of the amount of atomization gas on the mean diameter of the liquid droplets and the jet penetration. For

example, Lasheras et al. [11] found that, in open air, the Sauter mean diameter of the droplets produced at the centerline of a round water jet atomized by an annular air jet decreased when the amount of atomization gas was increased. For an internally-mixed spray nozzle, doubling the gas-to-liquid ratio resulted in a slightly deeper jet penetration into the bed, even though the corresponding mean droplet size measured in open air was nearly halved [12]. Another study conducted by Portoghese et al. [9], showed that increasing the GLR, atomization Gas to Liquid ratio in the injection nozzle, improved the spray quality but, depending on nozzle size and operating liquid flow rate, an optimum GLR could be identified beyond which any further increase in GLR had a negligible effect on nozzle performance.

Although several measuring techniques are available for assessing the moisture content of solid materials, especially in soils, such as Time domain reflectometry, neutron absorption, near-infrared reflectance (NIR), and microwave spectrometry [13, 14, 15-21], few were aimed at assessing the quality of the jet-bed interaction, i.e. the contact between injected liquid and fluidized particles, and those that did have not been tested for large scale fluid bed plant applications.

A technique was developed by Tsujimoto et al. [22], who employed an acoustic emission sensor in a fluidized bed granulator to detect unstable fluidization conditions, such as channelling and blocking, resulting from an excessive increase in solid moisture content. It was found that the propagation of the acoustic waves is attenuated by the presence of moisture in the bed solids. Significant changes in the mean acoustic emission amplitude, however, would require moisture levels higher than 15%, which precludes the use of this technique for adequate measurements of solid moisture during fluid bed drying. Book et al. [23] investigated passive acoustic and vibrometric methods just recently and proved that they can be used for the detection and monitoring of the changes of bed fluidity in a large scale fluid bed caused by much smaller moisture levels. Also, Chaplin et al. [24] recently showed how the S-statistic analysis could be applied to pressure fluctuation data measured in a fluid bed dryer to monitor the bed hydrodynamics during drying of pharmaceutical granules. This technique provides an early detection of the onset of entrainment taking place when the granule moisture content is about 11 wt. %, but not the means to monitor the evolution of the bed moisture content during drying.

Another technique was developed by McMillan et al. [25, 26] to assess the local quality of the liquid–solid mixing within the liquid jet cavity by measuring the local bed temperature at numerous locations in the jet region. While this method can be easily scaled up, it only measures the liquid–solid contact within the jet cavity.

In another study, Knapper et al. [27] injected a copper naphthenate tracer mixed with steam-atomized bitumen into a pilot plant coker and measured the copper concentration of coke samples to determine how well the injected bitumen had coated the fluidized coke particles. House et al. [3] examined the initial liquid–solid mixing by injecting a binder solution into a fluidized bed of coke particles. They stopped the fluidization gas shortly after the liquid injection, and allowed the liquid–solid agglomerates to slowly dry and solidify. The amount of liquid that contacted the coke particles during the injection was determined by analysis of the recovered agglomerates.

Some of other techniques have employed capacitance probes, which measure the electrical capacitance between two electrodes inserted in the soil, whose apparent dielectric constant is affected by the presence of interstitial water [18]. Capacitance probes are simple to set up and offer the advantage of providing instantaneous measurements of the soil water content.

Portoghese et al. [13, 9, 25, 14] used triboelectric probes to monitor changes in the wetted surface area of a fluidized bed produced by liquid injection via gas-atomized nozzles. A limitation of the triboelectric technique is that, since it measures a current generated by collisions of bed particles with an electrode, it is very sensitive to the local bed hydrodynamics whereas the conductance method is much less sensitive to the local bed hydrodynamics [28, 2].

Eventually the passive conductance method was implemented by Leach et al. [28], in which the conductance of the bed was measured after completing the liquid injection and defluidizing the wetted particles. The liquid, which is water, is more electrically conductive than the sand particles and a uniform distribution of the liquid on the particles maximizes the bed conductance. Therefore, a larger bed conductance indicates a more effective interaction of the liquid feed with the bed particles, i.e., a higher nozzle performance. The technique was then refined by Portoghese et al. [2], by applying a sinusoidal current to the fluidized bed and measuring the voltage drop across

the fluidized bed, in order to find its conductance. Leach et al. [1] used this technique to compare several gas-assisted liquid injection nozzles under a variety of operating conditions. All of these works were done using just a metal probe in one end of the bed.

The present paper intends to adapt and improve the previously developed experimental conductance method [1, 2] characterizing the effect of the atomization gas-to-liquid ratio (GLR) on the injected liquid distribution in a large fluidized bed, with a commercial-scale atomization nozzle. A new electrode configuration is employed to monitor the liquid distribution over the whole bed volume.

2.2 Apparatus

A schematic diagram and a picture of the trapezoidal shaped fluidized bed used in the present study is shown in Figure 2.1 and Figure 2.2. Water injections were atomized with nitrogen into the bed using a commercial-scale nozzle with the size and configuration as that of a fluid coker. The fluidized bed column had a trapezoidal cross-section of $3.5\text{m} \times 1.2\text{m} \times 0.2\text{m}$, and a height of 6.1 m to simulate one injection course of a Fluid Coker reactor (chosen based on previous jet expansion angle studies [8]), Figure 2.3. The internal length of 3.5 m was chosen based on a previous jet penetration study [29]. A diagram of the cross section of a typical commercial scale unit can be seen in Figure 2.4.

The atomization gas, nitrogen, was pre-mixed with pressurized water upstream of the nozzle conduit, in a bilateral flow conditioner (BFC); where water and nitrogen enter from opposite sides, both at an angle of 30° from the nozzle [30].

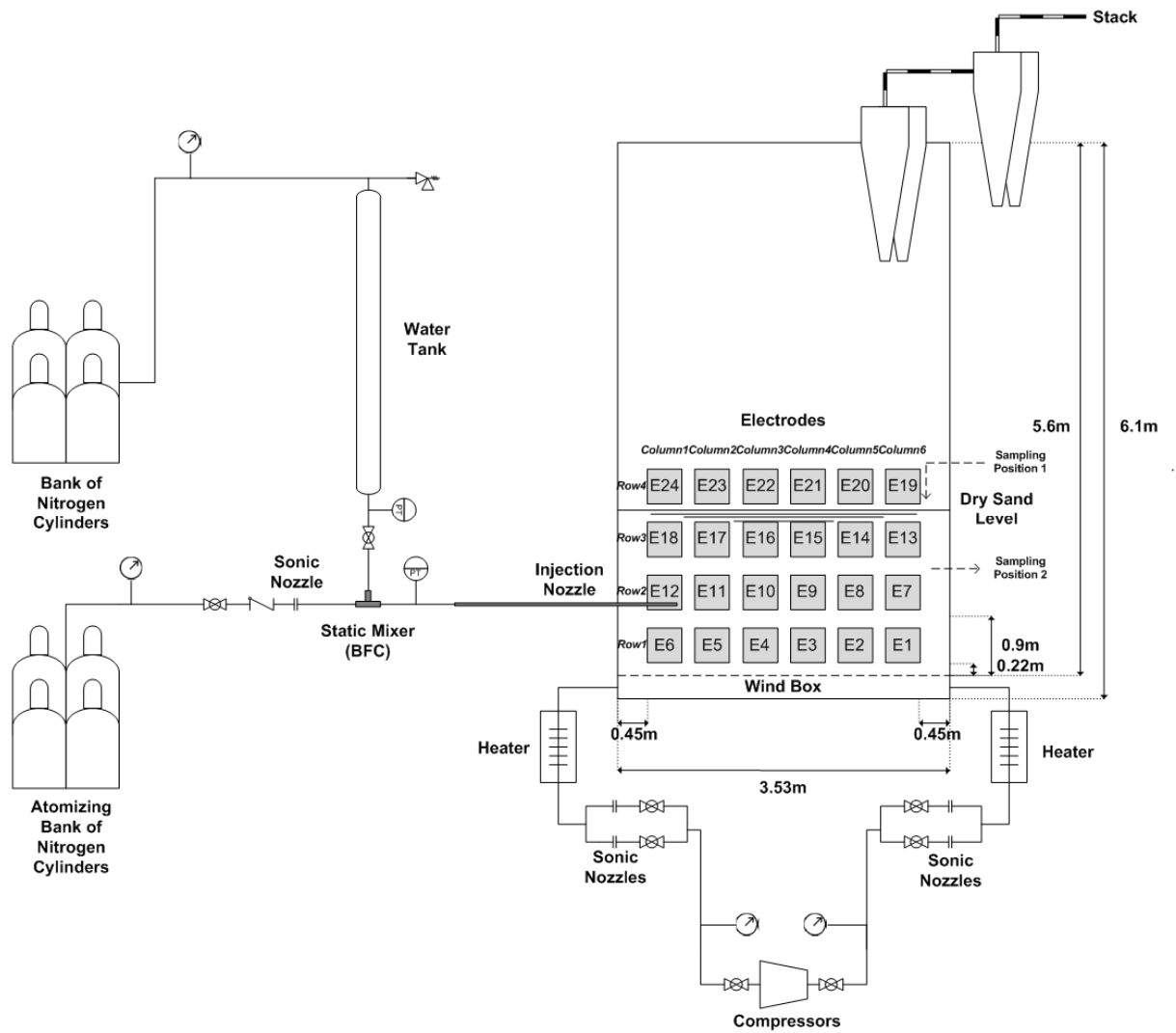


Figure 2.1 Schematic diagram of the experimental set-up



Figure 2.2 Experimental apparatus picture

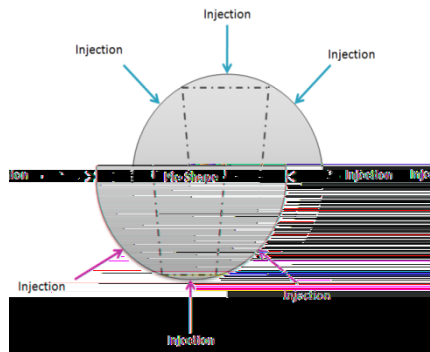


Figure 2.3 a Pie shaped slice cut out of the Fluid Coker cross section

The fluidized solid particles were silica sand particles with a Sauter-mean diameter of $150\ \mu\text{m}$ and an apparent particle density of $2650\ \text{kg/m}^3$ which were fluidized at a superficial gas velocity of $0.15\ \text{m/s}$. The particles are group B particles, using Geldart's powder classification system [31], and are not porous, as are the coke particles in Fluid Cokers. Sand is also nearly perfectly wettable with water, as coke is with bitumen in a fluid coker. In all the experiments performed the static bed height was approximately $1.85\ \text{m}$ above the distributor, and the total mass of solids in the bed was

about 7300 kg. Any entrained solids were returned to the bed through a system of internal and external cyclones placed in series.

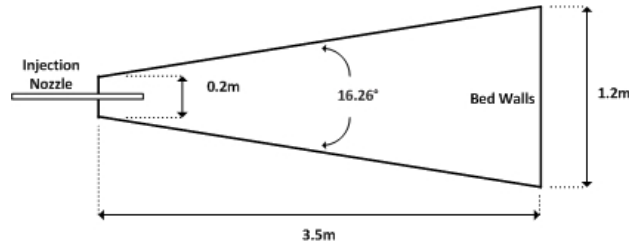


Figure 2.4 Top view of the bed

Five thermometers as well as two J-type thermocouples positioned at different locations along the width and the length of the bed, and another three thermocouples in the windbox, freeboard and secondary cyclones inlets helped ensure that the bed temperature was 22 °C at the start of each injection. Each one of the thermocouples penetrated 2 cm into the equipment to avoid significant stem losses.

The height of the bed was monitored from pressures measured with a large manometer using 5 pressure taps all placed in the centre of the wider end of the bed, at heights of 0.10, 0.89, 1.50, 2.11 and 3.93 m above the gas distributor.

A large nozzle was inserted 0.7 m into the bed about 0.9 m above the distributor grid, at the narrow end of the bed. The nozzle used in the tests used a geometry patented for commercial fluid cokers, Figure 2.5 [32].

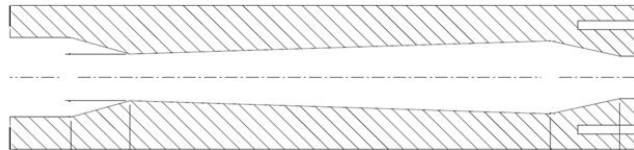


Figure 2.5 TEB Nozzle Scheme

Deionized water was used as the liquid to prevent the accumulation of impurities in the fluidized bed over the course of the experimental program. The mass flow rate of the atomization nitrogen was controlled using a pressure regulator upstream of a calibrated sonic nozzle. The liquid flow rate was regulated by pressurizing a liquid tank; for this study, the liquid flow rate was held constant at 1.47 kg/s, representing the commercial conditions. In order to keep it constant, nozzle calibration was done by doing open-air spray tests.

The pressure in the mixing region upstream of the nozzle as well as downstream of the water tank was also monitored. These measurements were taken to examine the effect of the required system pressure and the magnitude of pressure fluctuations on the quality of the liquid–solid contact in the bed and also to find the time of injection. These data were acquired at a rate of 50 Hz.

Twenty-four 0.245×0.245 m (10×10 inch) electrodes were installed along the length of the bed to measure the local bed conductance during the experiments. A linoleum sheet electrically insulated the electrodes from the steel bed walls, which were electrically grounded. A schematic diagram of the electrodes can be seen in Figure 2.1 and Figure 2.6.

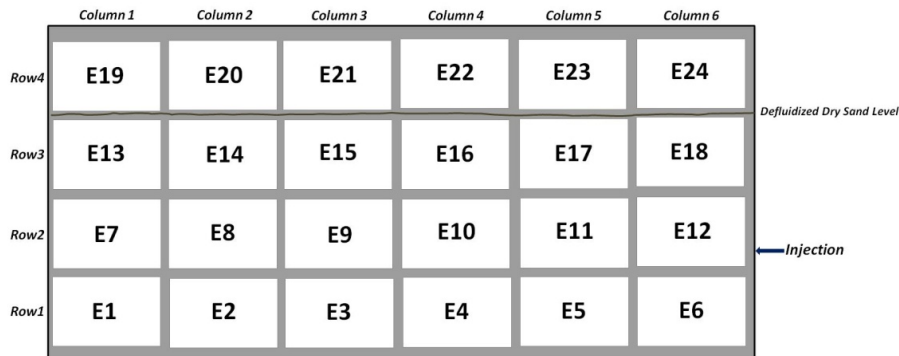


Figure 2.6 Schematic diagram of the electrodes configuration

An electrical AC sinusoidal signal, with a frequency of 100 Hz and a RMS voltage of 6.7 V, was created by a function generator. Applying this voltage across a series of measurement resistor, electrode, and bed material produced an electric current flowing between the electrode and the bed walls (I). For a given applied voltage (V1), and a given measurement resistance (Rm), the amplitude depends on the electrical properties of the bed material located between the electrode and the grounded bed walls. One can use the ratio of the voltage measured across the resistor (V2) to the voltage produced by the function generator (V1) to determine the bed conductance, using Ohm’s Law:

$$R_{bed} = \frac{1}{\Pi_{bed}} = R_m \left(\frac{V_1}{V_2} - 1 \right) \quad (1)$$

where Rbed is the electrical resistance of the bed, Π_{bed} is the electrical conductance of the bed and Rm is the measurement resistance (500 kΩ for all electrodes).

The voltages V1 and V2, as well as the thermocouples signals were recorded with a data acquisition system, at 1000 Hz for the voltages and at 3 Hz for the thermocouples. Figure 2.7 and Figure 2.8 show the equivalent circuit of the measurement system.

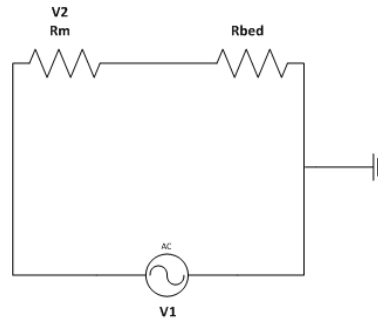


Figure 2.7 Circuit diagram of conductance technique

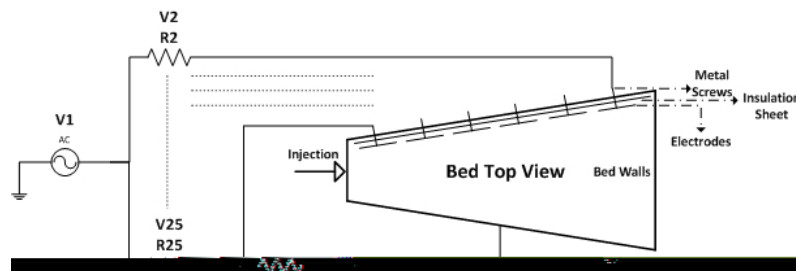


Figure 2.8 Schematic diagram of electrodes circuit

2.3 Experimental Procedure

2.3.1 Experiments procedure

Previous studies [9, 25, 14] have shown that conductance signals from a central rod electrode can be used to evaluate the effect of the atomization gas flow and of the spray nozzle geometry on the quality of the liquid–solid contacting in smaller fluidized beds. The technique used in this study, applies an electrical potential across the bed, and determines the electrical conductance of the bed material, which has been found to be related to the quality of the liquid distribution on the bed particles [1, 2, 3]. Twenty-four electrodes have been used in this study to monitor the moisture distribution at different locations throughout the bed and to provide more accurate measurements.

The silica sand particles used in this work have a very small electrical conductivity, but once they are wetted with water, water forms high conductivity paths. Moreover, if the water is well distributed throughout the particles, there will be a greater number of high conductivity paths, resulting in a higher bed conductance [1]. Maintaining fluidization for a short time after the liquid injection allows for settling, away from the electrode region, of the larger, wetter and, therefore, heavier liquid–solid agglomerates that may be formed upon the initial interaction of the liquid jet with the fluidized bed. Defluidizing the bed solids shortly after the liquid injection prevents the destruction of the wetter and larger agglomerates [28, 10]. It also prevents the signal noise due to the motion of the particles during fluidization [28].

The experimental procedure was as follows:

(1) The bed was fluidized before starting the injection for about 5 minutes with a fluidization air velocity of 0.15 m/s.

(2) 17 kg of water was then sprayed for approximately 11 seconds into the bed through the injection nozzle; this injection flow rate was similar to the flow rates used in commercial coking units.

(3) After the injection was completed, the bed was allowed to fluidize at 0.15 m/s for 34 s, and then at 0.06 m/s for an additional 45 s to allow the injected water to be mixed into the bed and for any large wet agglomerate to settle on the gas distributor.

(4) Afterwards the fluidization air was stopped, and the bed was defluidized for 9 minutes and 45 seconds.

(5) At last, the bed was re-fluidized at 0.15m/s for about 1 hour to dry. The drying end time was verified with the thermocouples.

Conductance measurements were performed over all the experiment period but the step (4) measurements were most important. Analysis of pressure measurements upstream of the spray nozzle determined that the transitory start-up period for the injection was very short, and could be neglected. Therefore, the water flow rate was assumed constant, at 1.47 kg/s, over the 11 seconds of injection in all experiments. Pressure measurements were taken, recording the pressure in the mixer. An example of these pressure measurements during the injection time can be seen in Figure 2.10. Preliminary calibration experiments determined the gas and liquid pressures required obtaining the same liquid flow rate for all the different GLR's (atomization Gas to Liquid Ratios) used in this study.

As a result, neglecting water evaporation during the injection time because of low injection time and also having low GLR, the overall liquid-to-solid mass ratio at the end of the liquid injection (L/S) was approximately 0.22 wt%. The tests were repeated with the same nozzle for the same conditions three times.

2.3.2 Calibration Experiments Procedure

Preliminary experiments determined that the injected liquid normally ended up as either free moisture, distributed in a thin layer around individual bed particles, or as moisture trapped within liquid-solid agglomerates. Testing showed that the liquid trapped within agglomerates had a negligible impact on the bed conductance, which depends primarily on the bed free moisture [1, 2].

Calibration experiments were used to determine the relationship between the local bed conductance and its free moisture. Different amounts of water were injected into the bed with a nozzle with a very high GLR of 36%, and providing enough mixing time to ensure that all the injected liquid ended up as free moisture, with no residual agglomerates.

The calibration experiments were performed as follows:

(1) The bed was fluidized before starting the experiment for about 5 minutes at a fluidization air velocity of 0.15 m/s.

(2) Then 9 kg of water with very high GLR of about 36% was sprayed into the bed through the injection nozzle.

(3) The fluidization air was stopped, and the bed was defluidized after 13 minutes, which is in fact after the peak of the conductance curve, since injection start, for approximately 2 minutes.

(4) The bed was re-fluidized at 0.15m/s and then after 1 minutes and 30 seconds defluidized again for a period of 2 minutes. Defluidization was done with the same time intervals 8 times in total.

(5) At last, re-fluidization at 0.15 m/s was done to dry the bed. Drying end time was verified by thermocouples.

Conductance measurements were performed continuously but only the defluidized bed measurements, in steps 3 and 4, were used for the calibration. To find out how much water is actually inside the sand bed, the amount of evaporated water was estimated as described in the Results section.

In order to verify that the bed is well mixed, or in other words the amount of free moisture is the same all over the bed after 13 minutes of mixing and an injection with a very high GLR, bed samples were taken after the first defluidization period. The moisture of the bed samples was measured using Karl Fisher. Table 2-1 shows a good agreement between the bed solid moisture content determined by titration (Using Karl-Fisher) and the real solid moisture content based on the amount of injected water in the well mixed experiment and the amount of evaporated water that was estimated by assuming that the air exiting the fluidized bed is completely saturated with water vapor. The samples were taken from two locations: the top window of the bed, which is near the top of the bed, and also mid-height in the wider end of the bed, as shown in Figure 1. The results confirm the assumption that the air leaving the bed is saturated with water vapor.

Sampling Position	Local Liq./Solid Ratio (Karl-Fisher)	Average Liq./Solid Ratio (Bed)
Window	0.00084482	0.00087945
Bed	0.00085163	0.00087945

Table 2-1 Remarkable agreement between the bed solid moisture found from sampling and the real one

2.4 Results

2.4.1 Variation of the bed conductance over the length of typical experiments

The conductance signals obtained from three duplicate experiments for a GLR of 2.24% are shown in Figure 2.9 (signals obtained with other GLRs had similar features). Under these conditions, liquid-solid agglomerates were formed. Each curve represents the average of the signals obtained from all the electrodes. All the injections started 126 s after the start of the signal acquisition, and were performed over a span of 11 s; it only took 5 s for the liquid to register on the first closest conductance electrode. The bed temperature was always adjusted to 22 °C before the injection.

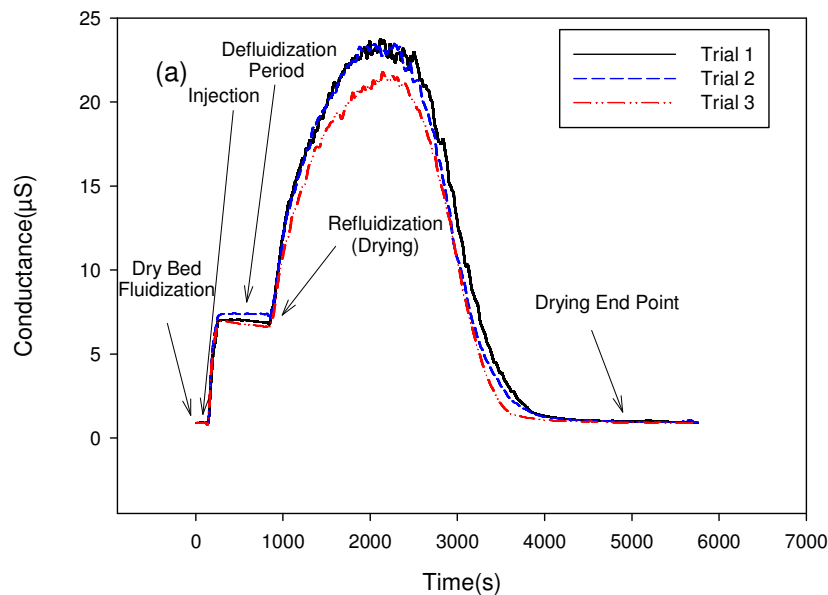


Figure 2.9 Conductance signal variation with time after the injections of GLR=2.24%. All the injections started at 126 s.

The conductance signal increases during the liquid injection, remains almost constant during the defluidization period, and then increases progressively upon refluidization until 2200 s, i.e. about 1355 s after the start of refluidization. It therefore took about twenty-two minutes for the liquid to spread enough to maximize the free moisture. Because of evaporation domination, the free moisture and the signal then decreased slowly until about 5000 s, the drying end point. Figure 2.9 thus shows that during refluidization, agglomerates are breaking up, generating additional free moisture, while free moisture disappears through evaporation; at first, the bed free moisture increases as the free moisture added through agglomerate breakup is greater than the free moisture disappearing through evaporation while, in the second part, the effect of evaporation predominates [1, 14].

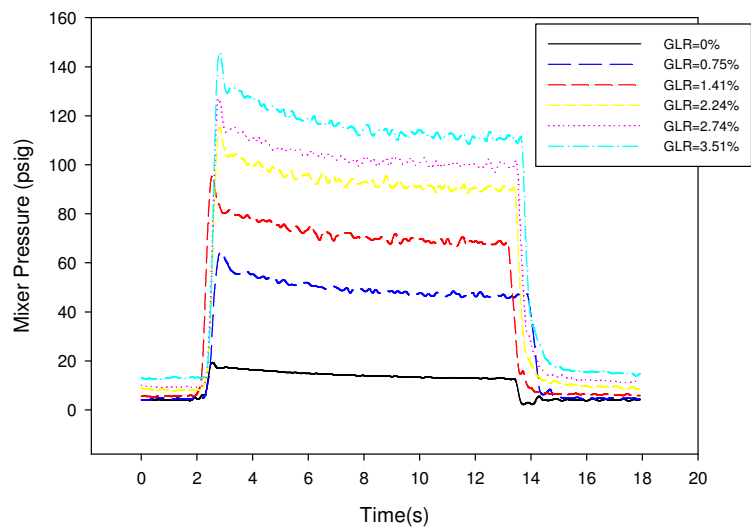


Figure 2.10 Pre-mixer pressure during injection for various GLR percentages from 0 to 3.5%, $m_{liq}=1.47$ kg/s

Figure 2.10 shows the variation with time of the pre-mixer pressure for different GLR's (or G/L ratio). The nozzle is the same as the commercial scale Fluid Coker nozzle for all of the cases and GLR percentage has been changed in the range of 0 to 3.5 percent having a rough interval of 0.75 percent. To achieve a higher GLR while keeping the liquid flowrate constant, the mixer pressure needs to be increased but its variation with GLR is non-linear, and preliminary experiments were required to set it at the appropriate value. The pressure decreases slightly over the course of injection. Figure 2.10 also shows that the injection time was essentially the same for all the GLR values.

2.4.2 Calibration experiments

Calibration experiments were performed with a GLR of 36%, to ensure that no agglomerates were formed. Each electrode was calibrated; Figure 2.11 shows a few typical calibration curves. Free moisture is the ratio of the mass of the total water detected by conductance to the mass of dry solids in the bed. For the calibration experiments, all the moisture was free moisture.

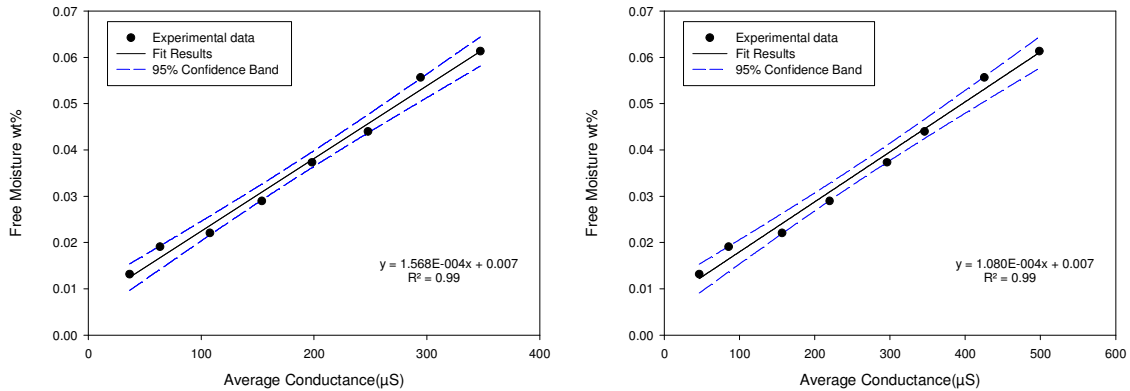


Figure 2.11 Left: Calibration curve of Electrode 9, Right: Calibration curve of Electrode 10

Assuming that the air exiting the fluidized bed is completely saturated with water vapor, by measuring its temperature, the mass of vaporized liquid could be estimated as a function of time. Measurements showed that the pressure above the bed was essentially atmospheric. Therefore, during fluidization after the injection and just before the defluidization stage, the humidity of the exiting air was derived from the measured bed and outlet temperatures, and the mass of evaporated liquid was deducted subsequently from the total mass of injected liquid, to determine the mass of water within the bed of sand at any time.

In order to verify the evaporation rate calculations, a dedicated experiment was performed with a smaller mass of injected liquid, 5.1 kg., to obtain results under conditions for which the free moisture was minimized. The data was recorded while the bed was fluidized at a superficial gas velocity of 0.15m/s. The drying end point was determined as shown in Figure 2.9. Table 2-2 shows that there was a very good agreement between the mass of injected water and the total calculated amount of

evaporated water during the entire experiment, using the temperature measurements and assuming that the air leaving the bed is saturated with water vapor.

Total injected liquid (gr)	Calculated amount of evaporated liquid (gr)
5100	4932

Table 2-2 Accordance between injected water and calculated evaporated water

2.4.3 Effect of GLR on injection quality

In order to get a more accurate estimate of the real average free moisture of the bed the bed geometry, as shown in Figure 2.12, was taken into account in the calculations via the following equation:

$$\text{Average free moisture} = \frac{\int_{x=0}^w \int_{y=0}^H f(x,y)L(x)dx dy}{H \int_{x=0}^w L(x)dx} \quad (2)$$

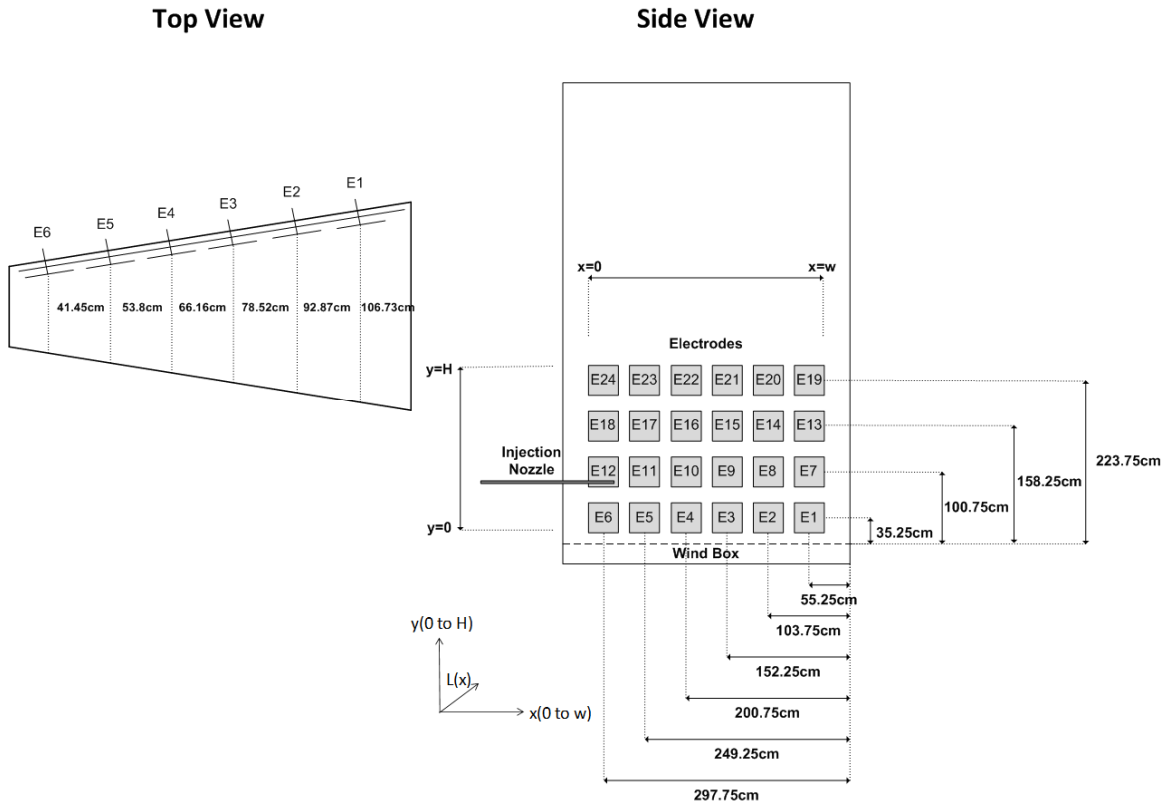


Figure 2.12 Coordinates of the electrodes in the bed

Where $f(x,y)$ is the free moisture in each 2D location of the bed that was found using Table Curve 3D software, implementing calibration curves, to fit the local

measurements of the free moisture and interpolate for any (x,y) location. This method assumes that the free moisture varies only over the coordinates x and y, which is a reasonable approximation. Accordingly, this correlation could be obtained:

$$\text{Average free moisture} = \frac{\sum_1^{N_x} (\sum_1^{N_y} f(x,y) * L(x))}{N_y * \sum_1^{N_x} L(x)} \quad (3)$$

$$\text{Average free moisture} = \frac{\sum_{j=1}^{N_x} (\sum_{i=1}^{N_y} f(x_j, y_i) * L(x_j))}{N_y * \sum_{j=1}^{N_x} L(x_j)} \quad (4)$$

Where $f(x_j, y_i)$ is the free moisture at the (x_i, y_i) location.

Figure 2.13 shows how the atomization GLR affected the average free moisture in the bed. The free moisture content is expressed in the weight percentage of bed free moisture obtained from calibration curves per total injected moisture. Thus it is defined as follow:

$$\tau = \frac{\text{Free moisture}}{\text{Total injected moisture}} * 100 = \frac{\left(\frac{\text{Mass of bed free water}}{\text{Mass of total dry solids}} \right)}{\left(\frac{\text{Mass of total injected water}}{\text{Mass of total dry solids}} \right)} * 100 \quad (5)$$

The figure indicates that the GLR range of 2.24 to 3.5 should be avoided since, over this range, increasing the atomization flowrate actually almost degrades the liquid distribution. It also shows that increasing the GLR to about 5.5% would be greatly beneficial since about two thirds of the injected liquid then becomes free moisture, instead of only one quarter for a GLR of about 1.5%.

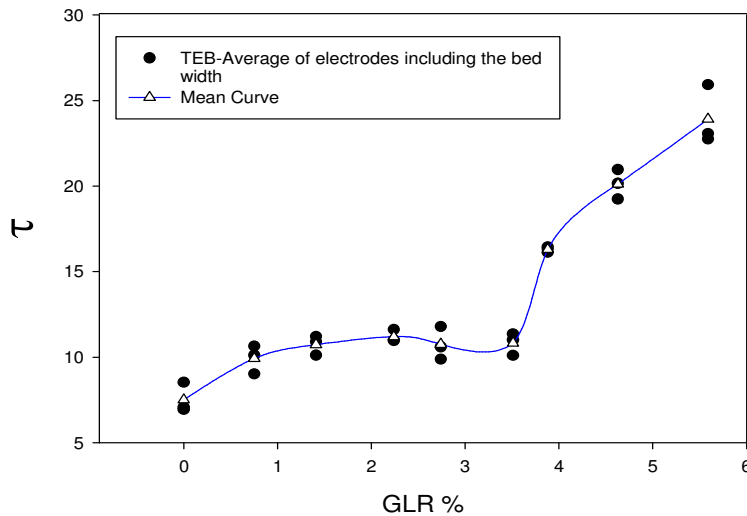


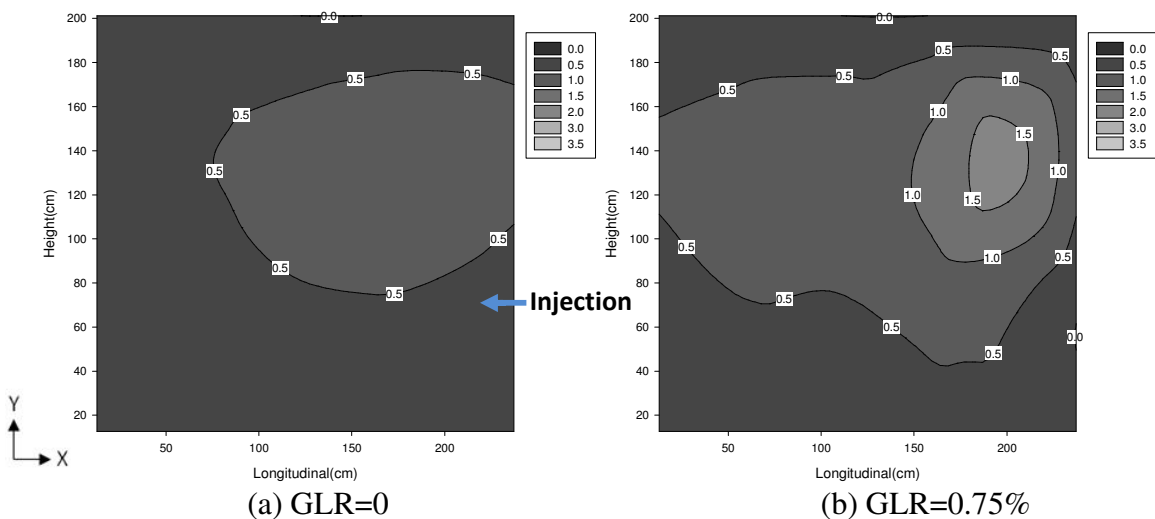
Figure 2.13 Effect of GLR on injection quality taking into account the width of the bed

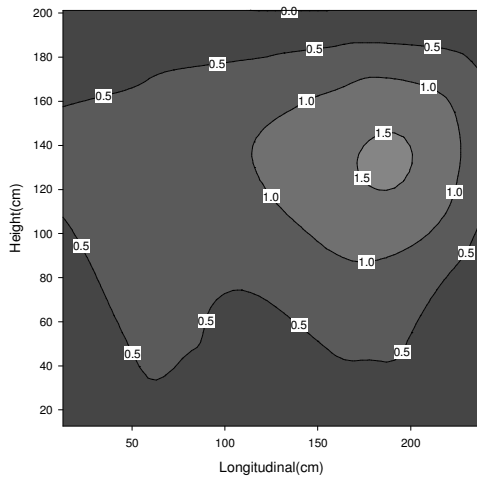
2.4.4 Effect of GLR on feed distribution across the bed

The free moisture at each specific location was determined from the individual electrode calibration equations. This made it possible to map the free moisture content, expressed in local τ , at various locations within the defluidized bed, as shown in Figure 2.14.

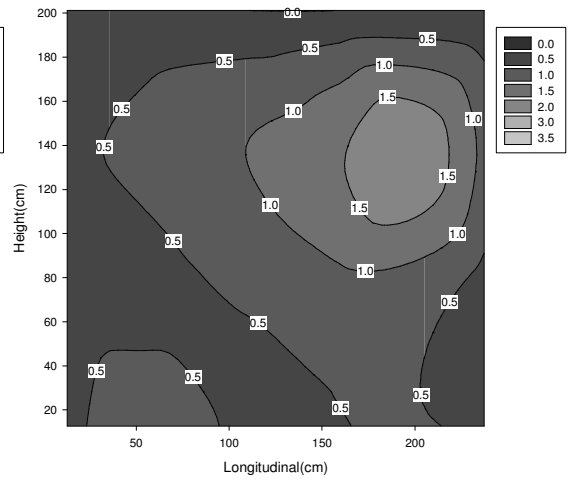
Figure 2.14 shows that, as the GLR is increased, the free moisture not only becomes greater, but it also becomes more uniformly distributed over the whole bed volume. As shown earlier, there is an exception for the GLR range of 2.24 to 3.51%, over which little improvement was observed. Increasing the GLR to 5.59% give much better results than at the commonly used GLR values of about 2%.

Figure 2.14 also shows that, for all the GLR values, the maximum free moisture concentration just after the injection was just above the nozzle tip. According to Ariyapadi et al. [8], most of the water trapped in agglomerates, on the other hand, goes to the tip of the jet cavity. The larger agglomerates tend to settle on the distributor and, in some cases such as for GLR values of 2.24%, 2.74% and 3.51%, one can see some free moisture near the grid and below the jet tip that was generated from the breakage of some of these large agglomerates.

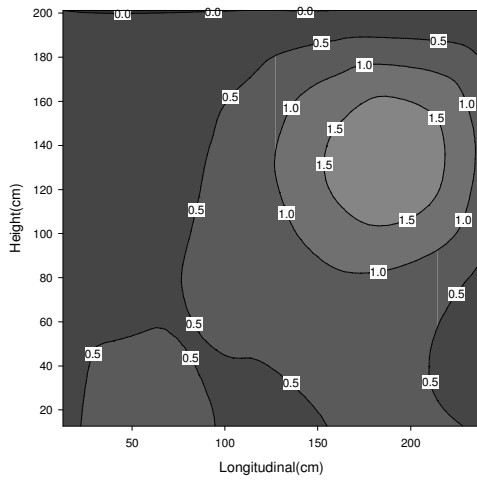




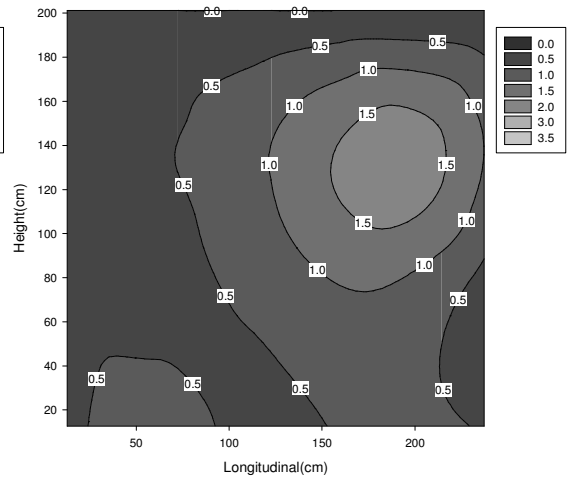
(c) GLR=1.41%



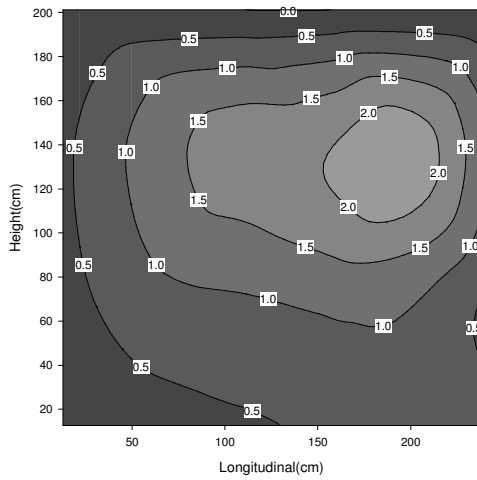
(d) GLR=2.24%



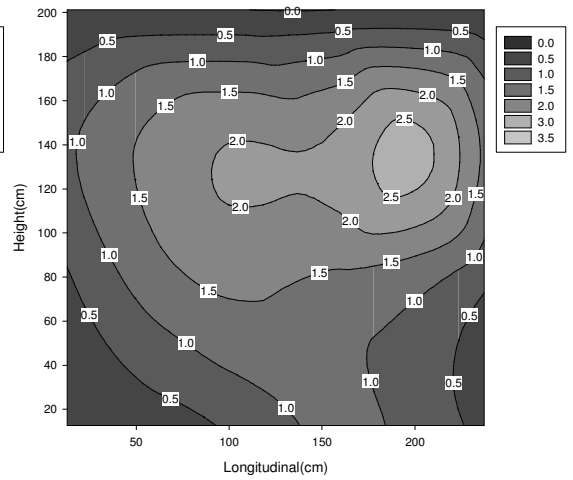
(e) GLR=2.74%



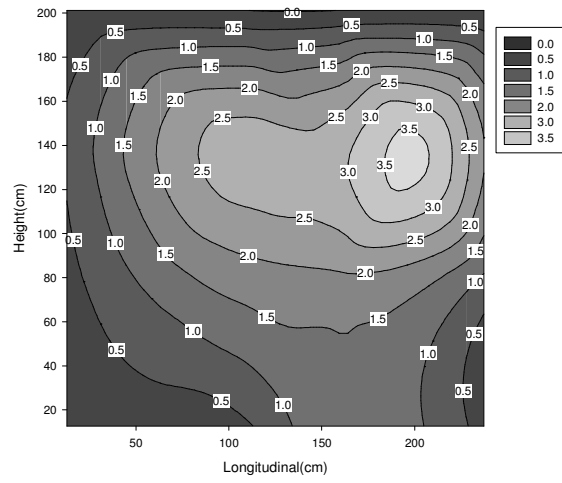
(f) GLR=3.51%



(g) GLR=3.88%



(h) GLR=4.63%



(i) $GLR=5.59\%$

Figure 2.14 Image of the bed for different GLR's (a to i); Z axis: Local τ

2.5 Conclusion

A new, conductance technique was successfully implemented in a large fluidized bed to assess the performance of an industrial scale fluid coker spray nozzle in terms of the quality of distribution of the liquid feed on the bed particles.

Operating at much higher atomization gas flowrates than commonly used would bring great benefits. It would not only dramatically reduce the amount of liquid trapped in agglomerates but would also distribute the liquid more uniformly over the whole bed volume.

2.6 Nomenclature

f	Free moisture
FCC	Fluid catalytic cracking
G/L	Gas-to-liquid mass ratio (wt%)
GLR	Gas-to-liquid mass ratio (wt%)
L	Width of the bed
L/S	Bed liquid-to-solid mass ratio (wt%)
NPI	Nozzle performance index (—)
N_x	Maximum of the length of the bed
N_y	Maximum of the height of the bed
R	Electrical resistance (Ω)
t	Time (s)
V_1	Voltage measured across function generator (V)
V_2	Voltage measured across resistor (V)
x	Length of the bed
y	Height of the bed

Greek Symbols

Π	Electrical conductance of fluidized bed (μS)
τ	Weight percentage ratio of free moisture over total injected moisture

2.7 References

1. Leach, A.; Chaplin, G.; Briens, C.; Berruti, F. Comparison of the performance of liquid–gas injection nozzles in a gas–solid fluidized bed. *Chemical Engineering and Processing: Process Intensification* **2009**, *48*, 780-788.
2. Portoghese, F.; House, P.; Berruti, F.; Briens, C.; Adamiak, K.; Chan, E. Electric conductance method to study the contact of injected liquid with fluidized particles. *AIChE J.* **2008**, *54*, 1770-1781.
3. House, P. K.; Saberian, M.; Briens, C. L.; Berruti, F.; Chan, E. Injection of a Liquid Spray into a Fluidized Bed: Particle–Liquid Mixing and Impact on Fluid Coker Yields. *Ind Eng Chem Res* **2004**, *43*, 5663-5669.
4. House P.; Berruti F.; Gray M.; Chan E.; Briens C.; Prediction of Propensity to Fouling in Fluid Cokers. AIChE National Meeting, San Francisco; November 12–17, **2006**.
5. Gray M.; Upgrading of petroleum residues and heavy oils. New York: Marcel Dekker, Inc; **1994**.
6. Leclere K.; Briens C.; Gauthier T.; Bayle J.; Bergougnou M.; Guigon P.; Liquid vaporization in a fluidized bed. *Ind Eng Chem Res.* **2001**; *40*:5415–5420.
7. Leclere K.; Briens C.; Gauthier T.; Bayle J.; Guigon P.; Bergougnou M.; Experimental measurement of droplet vaporization kinetics in a fluidized bed. *Chem Eng Proc.* **2004**; *43*:693–699.
8. Ariyapadi S.; Holdsworth D.; Norley C.; Berruti F.; Briens C.; Digital X-ray imaging technique to study the horizontal injection of gas-liquid jets into fluidized beds. *Int J Chem React Eng.* **2003**; *1*:A56.
9. Portoghese, F.; Ferrante, L.; Berruti, F.; Briens, C.; Chan, E. Effect of injection-nozzle operating parameters on the interaction between a gas–liquid jet and a gas–solid fluidized bed. *Powder Technol* **2008**, *184*, 1-10.
10. Weber, S.; Briens, C.; Berruti, F.; Chan, E.; Gray, M. Agglomerate stability in fluidized beds of glass beads and silica sand. *Powder Technol* **2006**, *165*, 115-127.
11. Lasheras J.C.; Villermaux E.; Hopfinger E.J.; Break-up and atomization of a round jet by a high-speed annular air jet, *J. Fluid Mech.* **1998** *357* 351–379.
12. Bruhns S.; Werther J.; An investigation of the mechanism of liquid injection into fluidized beds, *AIChE J.* **2005** *51* 766–775.
13. Portoghese, F.; Berruti, F.; Briens, C. Use of triboelectric probes for on-line monitoring of liquid concentration in wet gas–solid fluidized beds. *Chemical Engineering Science* **2005**, *60*, 6043-6048.
14. Portoghese, F.; Berruti, F.; Briens, C. Continuous on-line measurement of solid moisture content during fluidized bed drying using triboelectric probes. *Powder Technol* **2008**, *181*, 169-177.
15. Watano, S.; Sato, Y.; Miyanami, K. Application of fuzzy logic to moisture control in fluidized bed granulation, *Journal of Chemical Engineering of Japan* **28** (3) **1995** 282–287.

16. Gawande, N.A.; Reinhart, D.R.; Thomas, P.A.; McCreanor, P.T.; Townsend, T.G. Municipal solid waste in situ moisture content measurement using an electrical resistance sensor, *Waste Management* **23** **2003** 667–674.
17. Evett, S.R. Soil water measurement by time domain reflectometry, *Encyclopedia of Water Science* **2003** 894–898.
18. Starr, J.L.; Paltineanu, I.C. Soil water measurement by capacitance, *Encyclopedia of Water Science* **2003** 885–888.
19. Evett, S.R. Soil water measurement by neutron thermalization, *Encyclopedia of Water Science* **2003** 889–893.
20. Webster, J.G. The measurement, instrumentation and sensors handbook. Editor-in-Chief J.G. Webster, CRC Press in cooperation with IEEE Press, **1999** 72 pp. 11.
21. Watano, S.; Takashima, H.; Miyunami, K. Control of moisture content in fluidized bed granulation by neural network, *Journal of Chemical Engineering of Japan* **30** (2) **1997** 223–229.
22. Tsujimoto, H.; Yokoyama, T.; Huang, C.C.; Sekiguchi, I. Monitoring particle fluidization in a fluidized bed granulator with an acoustic emission sensor, *Powder Technology* **113** **2000** 88–96.
23. Book, G.; Albion, K.; Briens, L.; Briens, C.; Berruti, F. On-line detection of bed fluidity in gas–solid fluidized beds with liquid injection by passive acoustic and vibrometric methods. *Powder Technol* **2011**, *205*, 126–136.
24. Chaplin, G.; Pugsley, T.; Winters, C. The S-statistic as an early warning of entrainment in a fluidized bed dryer containing pharmaceutical granule, *Powder Technology* **149** **2005** 148–156.
25. Portoghese, F.; Berruti, F.; Briens, C.; Chan, E. Novel triboelectric method for characterizing the performance of nozzles injecting gas-atomized liquid into a fluidized bed. *Chemical Engineering & Processing: Process Intensification* **2007**, *46*, 924–934.
26. McMillan, J.; Zhou, D.; Ariyapadi, S.; Briens, C.; Berruti, F.; Chan, E. Characterization of the contact between liquid spray droplets and particles in a fluidized bed, *Ind. Eng. Chem. Res.* **44** **2005** 4931–4939.
27. Knapper, B.; Gray, M.; Chan, E.; Mikula, R. Measurement of efficiency of distribution of liquid feed in a gas–solid fluidized bed reactor, *Int. J. Chem. Reactor Eng.* **1** **2003**.
28. Leach, A.; Portoghese, F.; Briens, C.; Berruti, F. A new and rapid method for the evaluation of the liquid–solid contact resulting from liquid injection into a fluidized bed. *Powder Technol* **2008**, *184*, 44–51.
29. Ariyapadi, S.; Berruti, F.; Briens, C.; McMillan, J.; Zhou, D. Horizontal penetration of gas–liquid spray jets in gas–solid fluidized beds, *Int. J. Chem. React. Eng.* **2** **2004** Article A22.
30. McCracken, T.; Bennett, A.; Jonasson, K.; Kirpalani, D.; Tafreshi, Z.; Base, T.; Emberley, D.; Kennett, R.; Bulbuc, D.; Chan, E. Nozzle for Atomizing Liquid in Two Phase Flow. U.S. Patent 0001062 A1, **2005**.
31. Geldart, D. Types of gas fluidization. *Powder technol.* **7** **1973** 285.
32. Base, T.; Chan, E.; Kennett, R.; Emberly, D. Nozzle for Atomizing Liquid in Two Phase Flow. U.S. Patent 6003789, **1999**.

Chapter 3: Impact of draft tube on industrial-scale Fluid Coker spray jets in fluidized beds

3.1 Introduction

A large number of chemical and petrochemical processes such as Fluid Coking, fluid catalytic cracking (FCC) and gas-phase polymerization utilize liquid injection into a gas-solid fluidized bed. In industrial Fluid Cokers, bitumen is pre-mixed with atomization steam and then injected into a bed of solid coke particles, fluidized by steam and pre-heated to a temperature of about 550° C [1]. Atomizing the liquid with steam improves the liquid distribution leading to more rapid thermal cracking of the large hydrocarbon molecules of bitumen. Both the hydrocarbon conversion efficiency and the operability of the reactor are strongly affected by the initial contact between the injected liquid and the fluidized solids [2, 3, 4]. It has been shown that improving the contact of injected liquid with fluidized particles increases the yield of valuable liquid products in both the fluid catalytic cracking process, where most of the liquid is vaporizable, and in the fluid Coking process, where most of the liquid is not directly vaporizable, but must first be cracked to generate vaporizable fractions [2, 3, 5].

Several methods have been implemented to study the effect of the amount of atomization gas on the liquid and solid particles contact, [6, 7]. For example, a study conducted by Zirgachianzadeh et al.[8] in large scale and Portoghese et al. [9] in smaller scale, showed that increasing the atomization Gas to Liquid mass Ratio (GLR) improved the spray quality but, depending on nozzle size and operating liquid flow rate, an optimum GLR could be identified.

Mixing chambers are used in conjunction with nozzles in various industrial processes, to enhance liquid-solid mixing and consequently the liquid-solid contact. In this regard, a draft tube downstream of the nozzle was used by House et al. [3] to enhance the liquid distribution with a very small spray nozzle, with a liquid flowrate of the order of 1 l/min. Several studies were also performed with small spray nozzles.

The effect of various draft tube geometry and location on the solids entrainment rate into the spray jet cavity was also investigated by Hulet et al. [10]. They showed that

there is an optimum distance between the spray nozzle and the draft tube, which occurs when the jet hits the draft tube wall within the inlet section of the tube.

McMillan et al. [11] determined the quality of the solid-liquid mixing with an assembly of fast response thermocouples, located downstream of the gas-liquid spray jet, that provided instantaneous temperature readings over the liquid spray jet cross section at different axial positions along the length of the jet. They showed that very good and rapid contact between sprayed droplets and particles can be achieved by using a draft tube mixer comparing to not using it. The results also show that the liquid is not well-distributed before contacting the draft tube, in the original free jet, but improves after it comes into contact with the draft tube wall and the mixing improves significantly along the tube. The distance between nozzle tip and draft tube that provided the best mixing performance occurred when the jet impacted the draft tube wall 0.8 tube diameters into the length of the tube, as was also found by Hulet et al. [10].

Ariyapadi et al. [12] hypothesized that the draft tube aids in the formation of large eddies that intensify mixing, and built a model based on this mixing enhancement [13]. Preliminary analysis indicated that the jet penetration distances for the smaller diameter tube scenario was slightly lower than both the 1.9 cm dia. draft tube case and the free jet case, revealing the fact that the energy may have been dissipated due to the mixing and/or frictional losses.

None of the above studies were performed with spray nozzles of a realistic size, since commercial scale typically have liquid flowrates in the range of 100 l/min, i.e. two orders of magnitude higher than the flowrates used in previous studies. This was due to the difficulty of performing measurements with large spray nozzles. Zirgachianzadeh et al. [8] have recently developed a new method to measure the quality of the liquid distribution on the fluidized particles for commercial-scale spray nozzles. Zirgachianzadeh et al. [8] showed that the quality of the liquid distribution was greatly affected by the atomization gas flowrate.

The objective of the present paper is, therefore, to evaluate the effect of the enhanced solids entrainment (ESE) device, comprising of a cylindrical draft tube installed downstream of the nozzle, on the distribution of liquid sprayed into a fluidized

bed with a commercial size nozzle. This evaluation will be performed over a wide range of atomization gas flowrates.

3.2 Apparatus

The fluidized bed used in the present study is the same as the one used in the previous study the only difference being the cylindrical draft tube installed downstream of the nozzle, [8], as it shown in Figure 3.1 and Figure 3.2. Water injections were atomized with nitrogen into the bed using a commercial-scale nozzle with the size and configuration as that of a fluid coker.

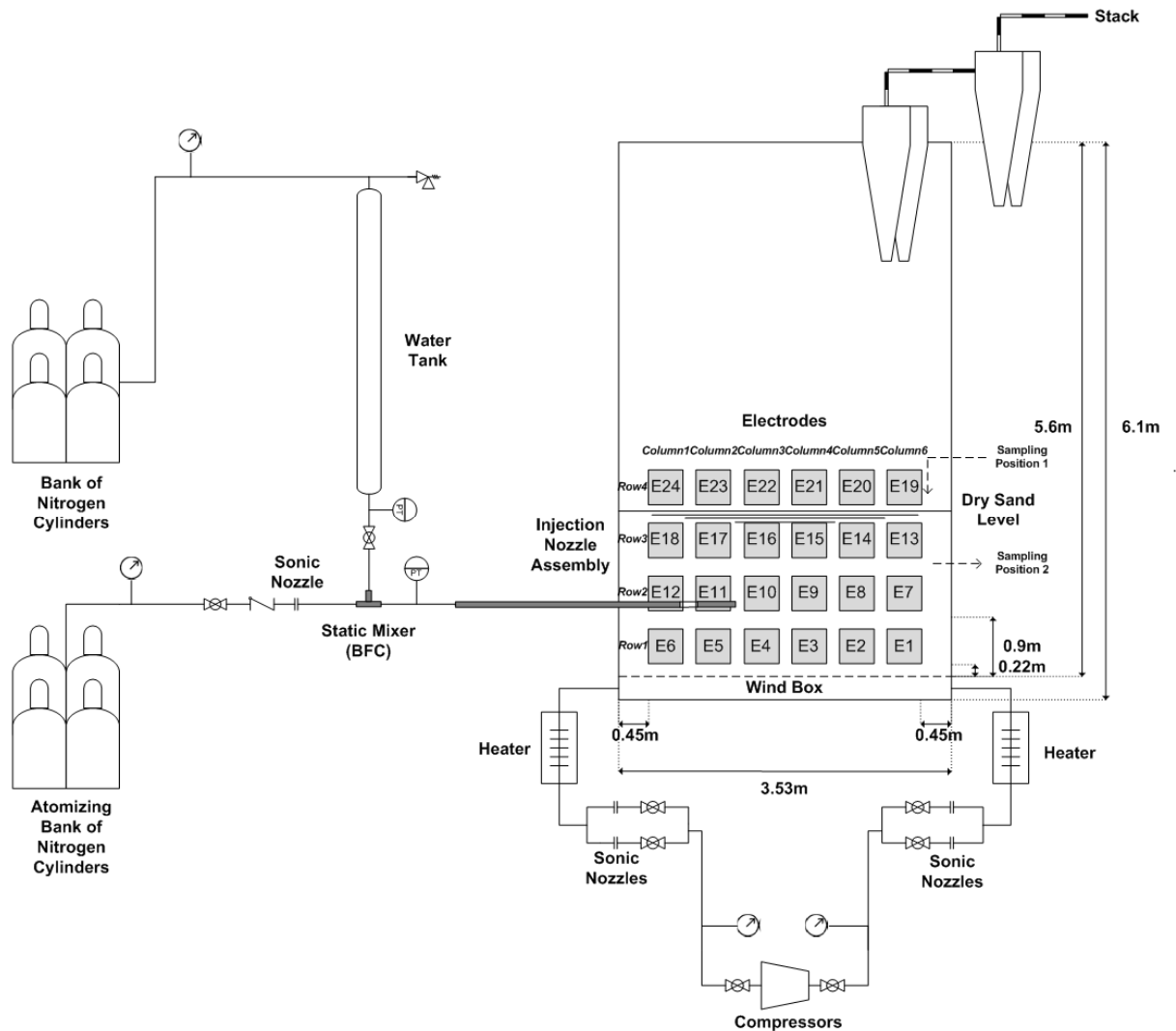


Figure 3.1 Schematic diagram of the experimental set-up



Figure 3.2 Experimental apparatus picture

The fluidized bed column had a trapezoidal cross-section of $3.5\text{m} \times 1.2\text{m} \times 0.2\text{m}$, and a height of 6.1 m to simulate one injection course of a fluid coker reactor (chosen based on previous jet expansion angle studies [14]), Figure 3.3.

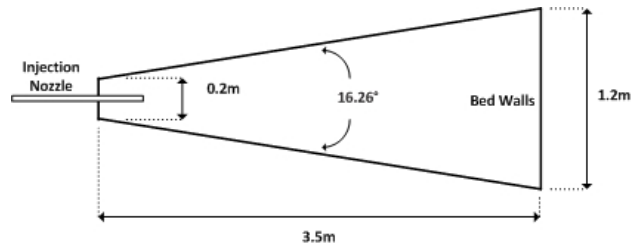


Figure 3.3 Top view of the bed

The large nozzle assembly was inserted 1.2m into the bed about 0.9 m above the distributor grid, at the narrow end of the bed. A protection tube was also installed around the nozzle and the pipe upstream of it to protect them from breaking. The atomization gas was pre-mixed with pressurized water upstream of the nozzle conduit, in a bilateral flow conditioner (BFC) [15]. The nozzle used in the tests used a geometry patented for commercial Fluid Cokers [16], Figure 3.4.

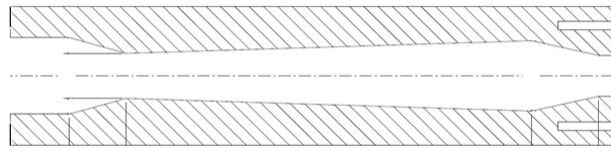


Figure 3.4 TEB Nozzle Scheme

A cylindrical draft tube was mounted coaxially, downstream of the spray nozzle, Figure 3.5. The internal diameter (D) of the draft tube was 103 mm and the length (L) was 380 mm. The distance from the nozzle exit to the draft tube was kept constant at 137 mm which was chosen based on the optimum distances found by Jennifer et al. and Hulet et al. [10, 11].

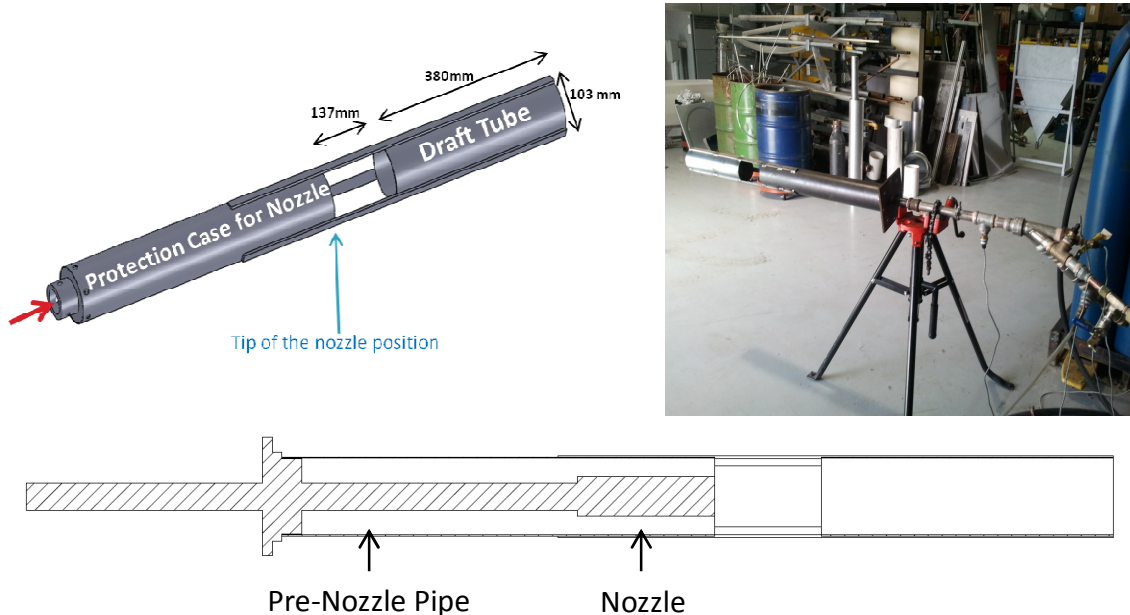


Figure 3.5 Nozzle Assembly Scheme (ESE)

The fluidized solid particles were Silica sand particles with the same characteristics as the ones used by previous study [8]. The total mass of solids in the bed was about 7300 kg and the temperature was 22 °C.

Twenty-four 0.245×0.245 m (10×10 inch) electrodes were installed along the length of the bed to measure the local bed conductance during the experiments. A schematic diagram of the electrodes can be seen in Figure 3.1.

The electrical set-up was exactly the same as the one used by Zirgachianzadeh et al.[8].

3.3 Experimental Procedure

3.3.1 Experiments procedure

Previous study [8] has shown that the conductance signals from twenty four electrodes installed on the bed could be used to map the moisture distribution across the bed. Defluidizing the bed solids shortly after the liquid injection prevents the destruction of the wetter and larger agglomerates [17, 18]. It also prevents the signal noise due to the motion of the particles.

The experimental procedure was as follows:

(1) The bed was fluidized before starting the injection for about 5 minutes with a fluidization air velocity of 0.15 m/s.

(2) 17 kg of water was then sprayed for approximately 11 seconds into the bed through the injection nozzle; this injection flow rate was similar to the flow rates used in commercial coking units.

(3) After the injection was completed, the bed was allowed to fluidize at 0.15 m/s for 34 s, and then at 0.06 m/s for an additional 45 s to allow the injected water to be mixed into the bed and for any large wet agglomerate to settle on the gas distributor.

(4) Afterwards the fluidization air was stopped, and the bed was defluidized for 9 minutes and 45 seconds.

(5) At last, the bed was re-fluidized at 0.15m/s for about 1 hour to dry. The drying end time was verified with the thermocouples.

Conductance measurements were performed over all the experiment period but the step (4) measurements were most important. Therefore, the water flow rate was assumed constant, at 1.47 kg/s, over the 11 seconds of injection in all experiments.

The overall liquid-to-solid mass ratio at the end of the liquid injection (L/S) was approximately 0.22 wt% and the tests were repeated with the same nozzle for the same conditions three times.

3.3.2 Calibration Experiments Procedure

Calibration curves used in this study are exactly the same as the ones used by Zirgachianzadeh et al. [8]. Testing showed that the liquid trapped within agglomerates had a negligible impact on the bed conductance, which depended solely on the bed free moisture.

Calibration experiments were used to determine the relationship between the local bed conductance and its free moisture. Different amounts of water was injected into the bed with a nozzle with a very high GLR of 36%, and providing enough mixing time to ensure that all the injected liquid ended up as free moisture, with no residual agglomerates.

The calibration experiments were performed as follows:

(1) The bed was fluidized before starting the experiment for about 5 minutes at a fluidization air velocity of 0.15 m/s.

(2) Then 9 kg of water with very high GLR of about 36% was sprayed into the bed through the injection nozzle.

(3) The fluidization air was stopped, and the bed was defluidized after 13 minutes, which is in fact after the peak of the conductance curve, since injection start, for approximately 2 minutes.

(4) The bed was re-fluidized at 0.15m/s and then after 1 minutes and 30 seconds defluidized again for a period of 2 minutes. Defluidization was done with the same time intervals 8 times in total.

(5) At last, re-fluidization at 0.15 m/s was done to dry the bed. Drying end time was verified by thermocouples.

In order to verify that the bed is well mixed, bed samples were taken after the first defluidization period. The moisture of the bed samples was measured using Karl Fisher. Table 3-1 shows a good agreement between the bed solid moisture content determined by titration (Using Karl-Fisher) and the real solid moisture content.

Sampling Position	Local Liq./Solid Ratio (Karl-Fisher)	Average Liq./Solid Ratio (Bed)
Window	0.00084482	0.00087945
Bed	0.00085163	0.00087945

Table 3-1 Remarkable agreement between the bed solid moisture found from sampling and the real one

3.4 Results

3.4.1 Calibration

Calibration of each electrode was the same as the one used in the previous work, [8]; Figure 3.6 shows a few typical calibration curves. Free moisture is the ratio of the mass of the total water detected by conductance to the mass of dry solids in the bed. For the calibration experiments, all the moisture was assumed to be free moisture as the used GLR was very high and enough time was given for a complete mixing.

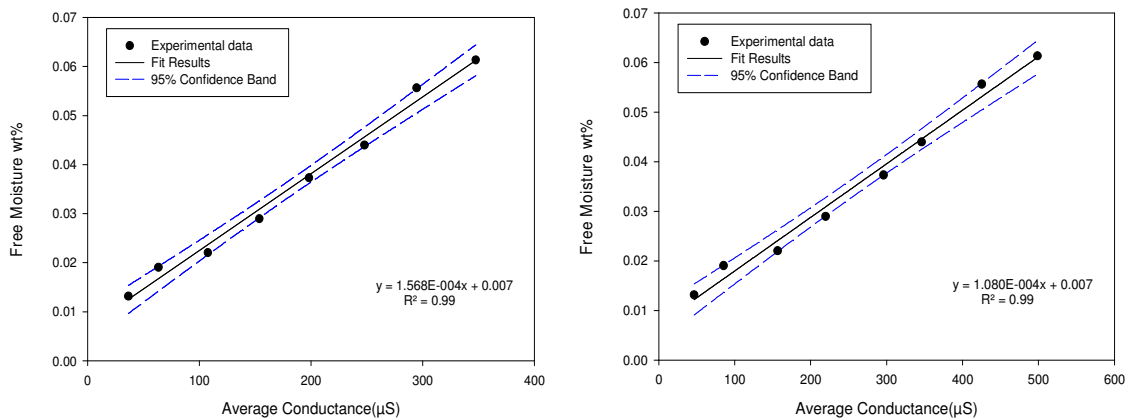


Figure 3.6 Left: Calibration curve of Electrode 9, Right: Calibration curve of Electrode 10

In order to verify the evaporation rate calculations, a dedicated experiment was performed with a smaller mass of injected liquid, 5.1 kg., to obtain results under conditions for which the free moisture was minimized. The data was recorded while the bed was fluidized at a superficial gas velocity of 0.15m/s. Table 3-2 shows that there was a very good agreement between the mass of injected water and the total calculated amount of evaporated water.

Total injected liquid (gr)	Calculated amount of evaporated liquid (gr)
5100	4932

Table 3-2 Accordance between injected water and calculated evaporated water

3.4.2 Comparison of ESE and Free Jet in terms of injection quality

The average free moisture was obtained by averaging all free moistures that were obtained from each electrode since, under these conditions, the bed was not well mixed. Like what happened with the free jet in the previous study [8], even for ESE the free moisture increased with increasing GLR with the exception of the range of 2.24 to 3.51%, where the free moisture did not vary with the GLR, Figure 3.7. In this figure, free moisture definition is the same as in Figure 3.6 and the total injected moisture is the mass of total injected water divided by the mass of total dry solids.

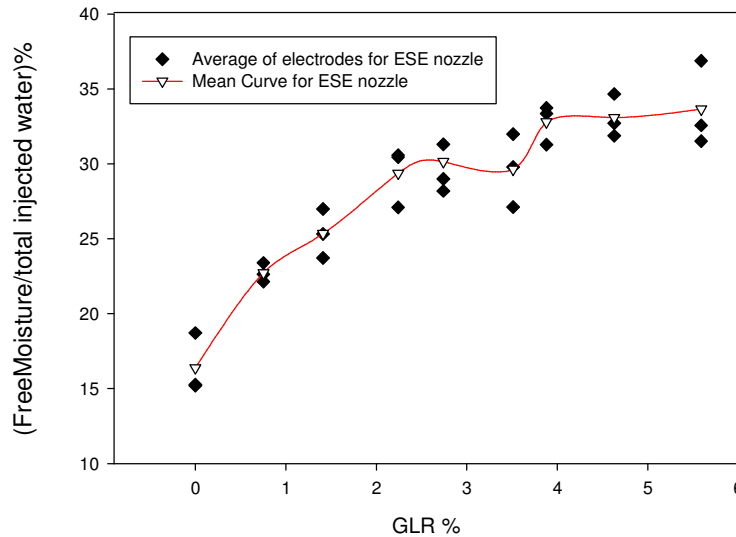


Figure 3.7 Effect of GLR on injection quality with ESE nozzle

In order to get a more accurate estimate of the real average free moisture of the bed, the 3D dimensions of the bed, as shown in Figure 3.8, must be included in the calculations via the following equation:

$$\text{Average free moisture} = \frac{\int_{x=0}^W \int_{y=0}^H f(x,y)L(x)dx dy}{H \int_{x=0}^W L(x)dx} \quad (1)$$

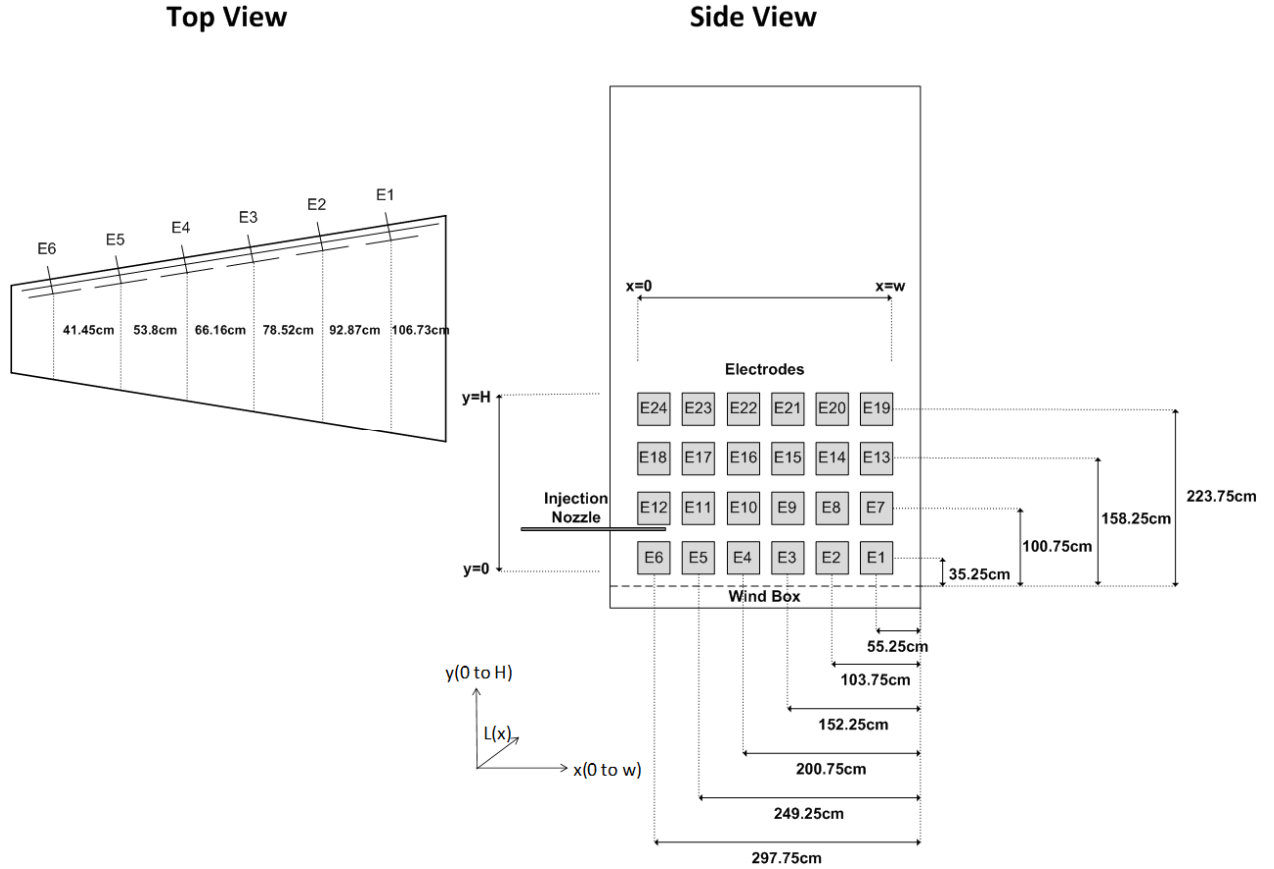


Figure 3.8 Coordinates of the electrodes in the bed

Where $f(x,y)$ is the free moisture in each 2D location of the bed that was found using Table Curve 3D software. Accordingly, this correlation could be obtained:

$$\text{Average free moisture} = \frac{\sum_1^{Nx} (\sum_1^{Ny} f(x,y) * L(x))}{Ny * \sum_1^{Nx} L(x)} \quad (2)$$

$$\text{Average free moisture} = \frac{\sum_{j=1}^{Nx} (\sum_{i=1}^{Ny} f(x_i, y_i) * L(x_i))}{Ny * \sum_{j=1}^{Nx} L(x_j)} \quad (3)$$

Where $f(x_j, y_i)$ is the free moisture amount in every 2D location of the bed, which was found using Table Curve 3D; as the equation is different for each GLR they have not been mentioned here. This method assumes that the free moisture varies only over the coordinates x and y , which is a reasonable approximation. Afterwards, knowing the width of the bed in each electrode position, $L(x_j)$, the curve of the average free moisture including the width of the bed could be drawn, Figure 3.9.

Figure 3.9 displays the privilege of using ESE over free jet, however it also indicates that ESE effect is larger for lower GLR's comparing to very high GLR's and emphasizes the optimum range of the nozzle. A low pressure profile is formed in front of

the draft tube entrance which entrains bed particles into the tube. In fact, the draft tube works as mixing chamber for the particles and enhances the contact between entrained particles and liquid droplets. The free moisture content is expressed in the weight percentage of bed free moisture, obtained from calibration curves, per total injected moisture. It is expressed as follow:

$$\tau = \frac{\text{Free moisture}}{\text{Total injected moisture}} * 100 = \frac{\left(\frac{\text{Mass of bed moisture}}{\text{Mass of total dry solids}}\right)}{\left(\frac{\text{Mass of total injected water}}{\text{Mass of total dry solids}}\right)} * 100 \quad (4)$$

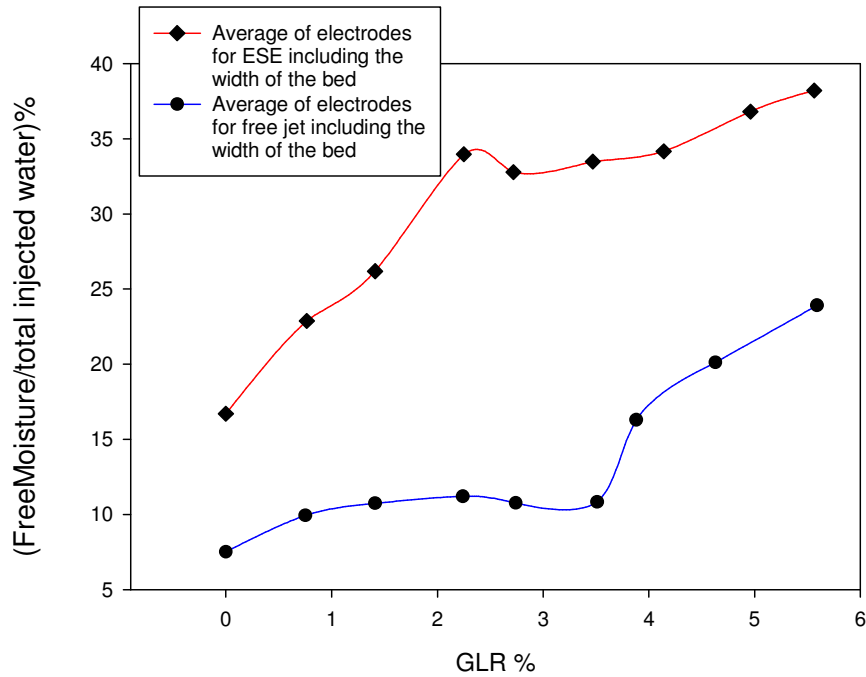


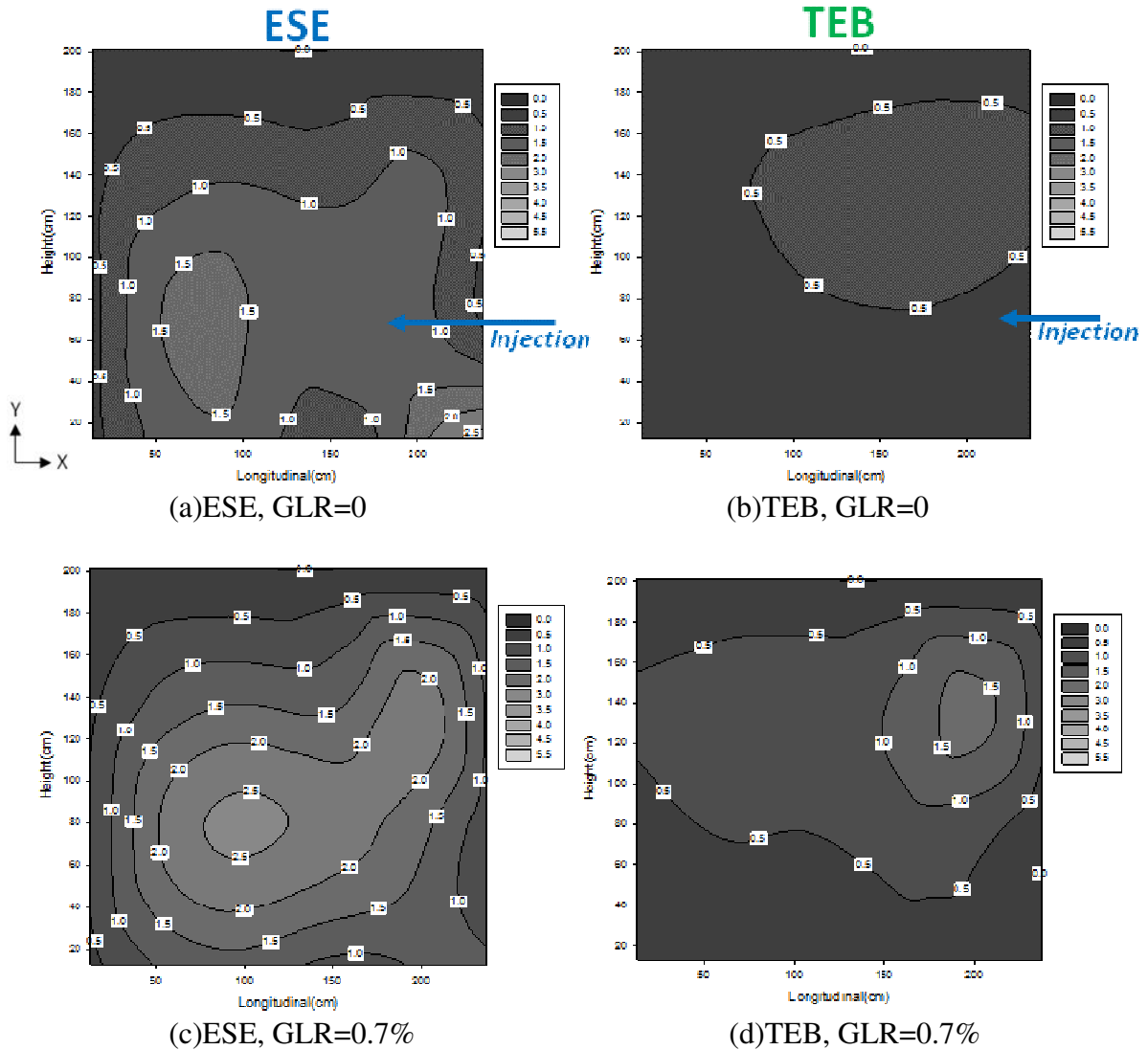
Figure 3.9 Effect of GLR on injection quality taking into account the width of the bed for ESE nozzle

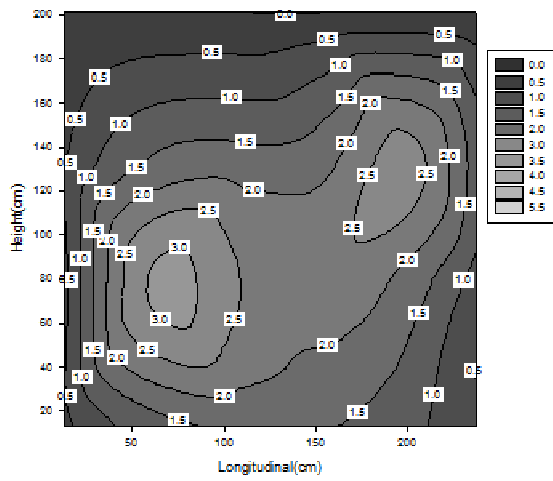
3.4.3 Comparison in terms of feed distribution across the bed

Individual electrode calibration equations mentioned previously helped finding the free moisture in each specific location of the bed. Accordingly the bed was mapped based on its free moisture content distribution, expressed in local τ , at various locations within the defluidized bed. It gave the amazing advantage of being able to compare moisture distribution using ESE and free jet across the bed, as shown in Figure 3.10.

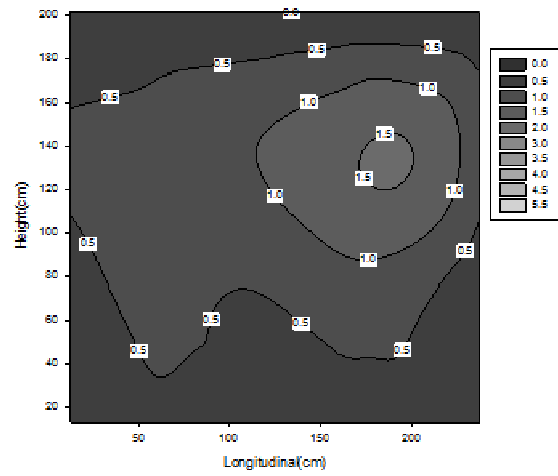
Like what had been shown in the previous work [8] for free jet, both the free moisture and liquid distribution is incredibly improved with GLR increase, Figure 3.10.

However, still there is an exception for the GLR range of 2.24 to 3.51%, over which little improvement was observed. Increasing the GLR to 5.59% gives a better result than that of the commonly used GLR values of about 2%. Furthermore, in comparison to free jet, ESE has a much better liquid distribution with respect to free jet in all GLR's and without reducing the liquid distribution in other areas, ESE has greatly improved the jet penetration through the bed.

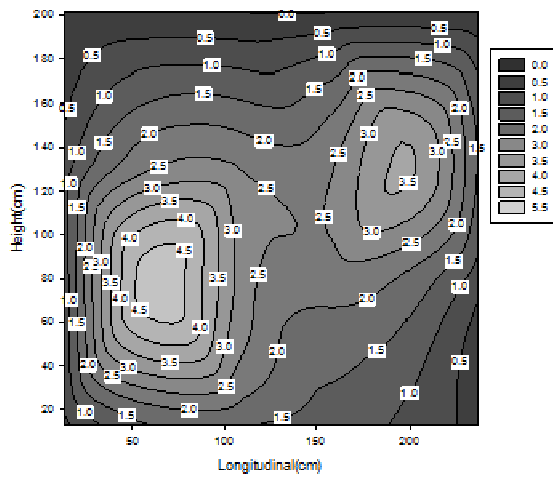




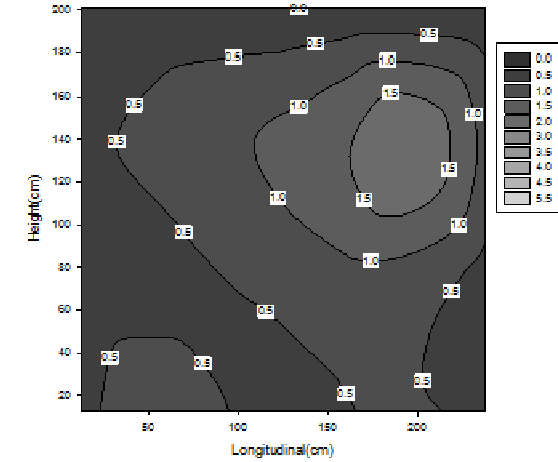
(e)ESE, GLR=1.4%



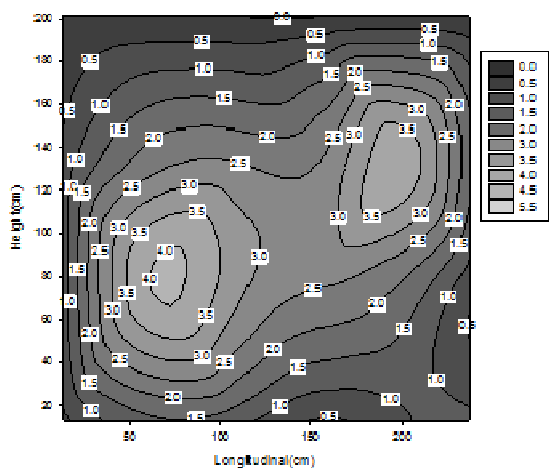
(f)TEB, GLR=1.4%



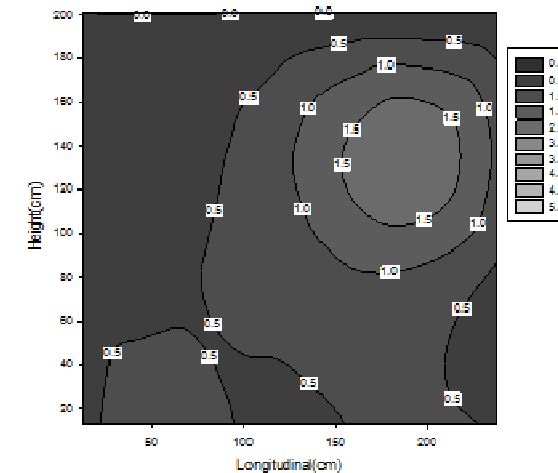
(g)ESE, GLR=2.2%



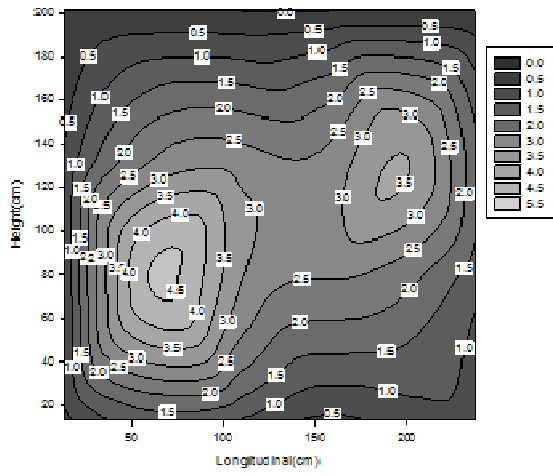
(h)TEB, GLR=2.2%



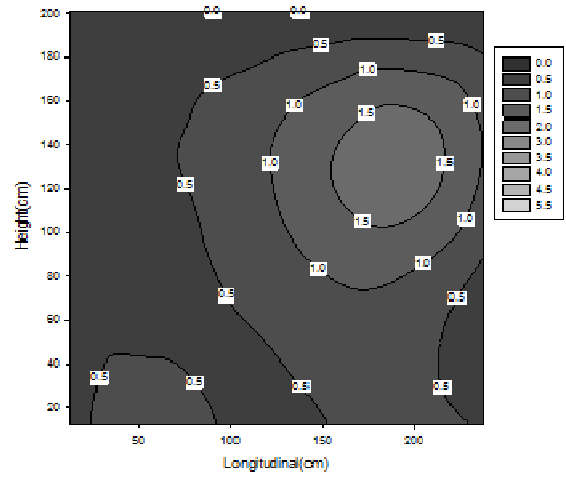
(i)ESE, GLR=2.7%



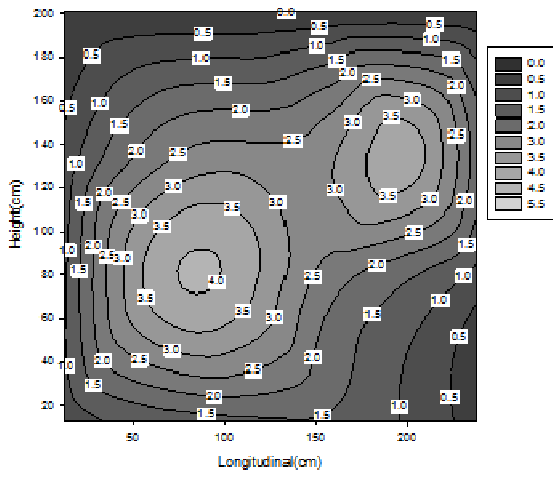
(j)TEB, GLR=2.7%



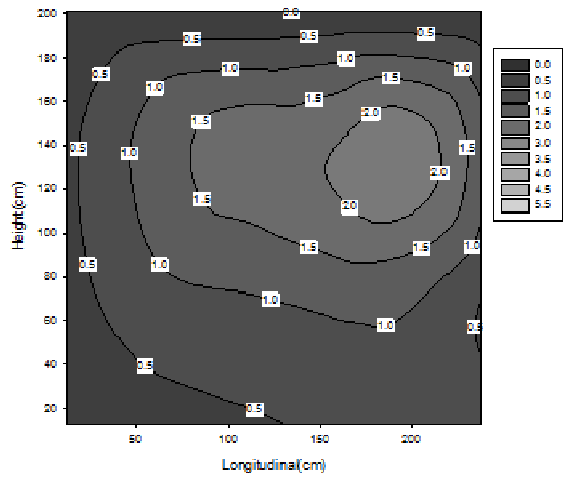
(k)ESE, GLR=3.4%



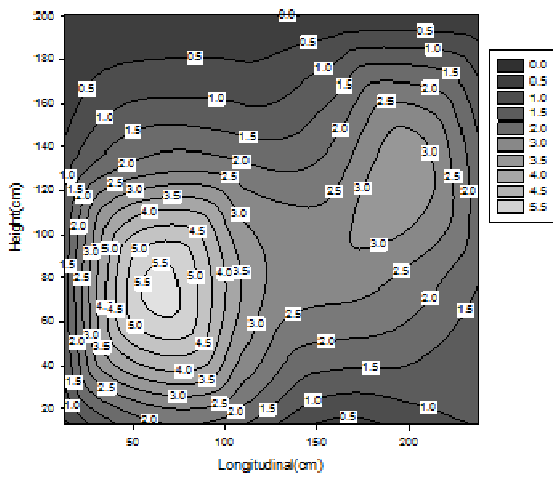
(l)TEB, GLR=3.5%



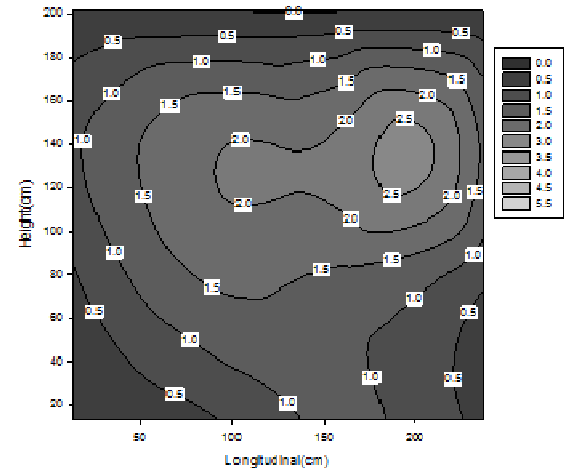
(m) GLR=4.1%



(n) GLR=3.8%



(o)ESE, GLR=4.9%



(p)TEB, GLR=4.6%

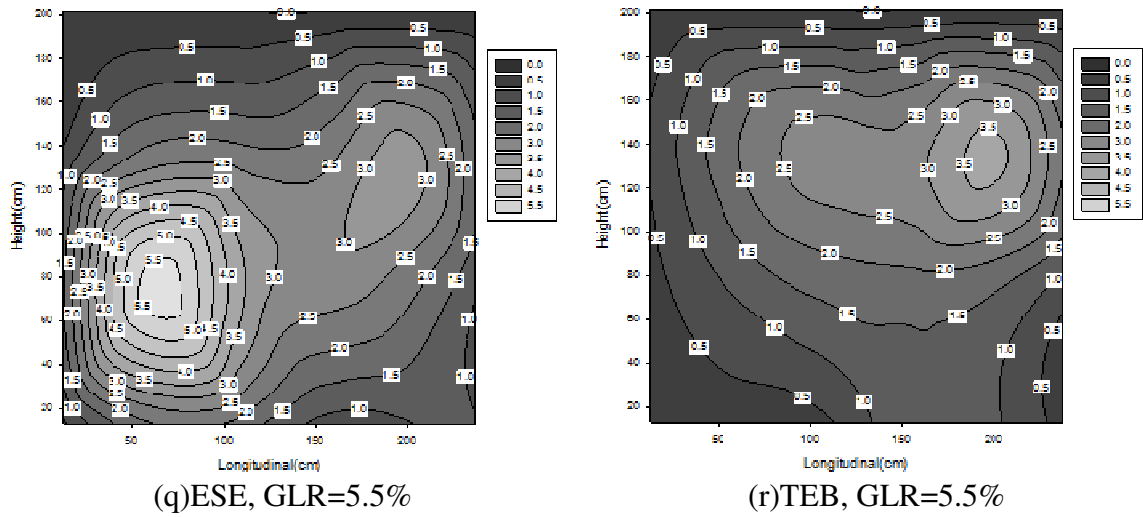


Figure 3.10 Comparison of images of the bed for ESE and TEB nozzles for different GLR's (a to r)

Left images: ESE nozzle; Right Images: TEB nozzle. Z axis: Local τ

Moreover, according to Figure 3.9, injection quality of GLR=0 of ESE is impressively equal to that of GLR=3.8 in a regular TEB nozzle. In Figure 3.11 , the moisture distribution of these two cases is compared.

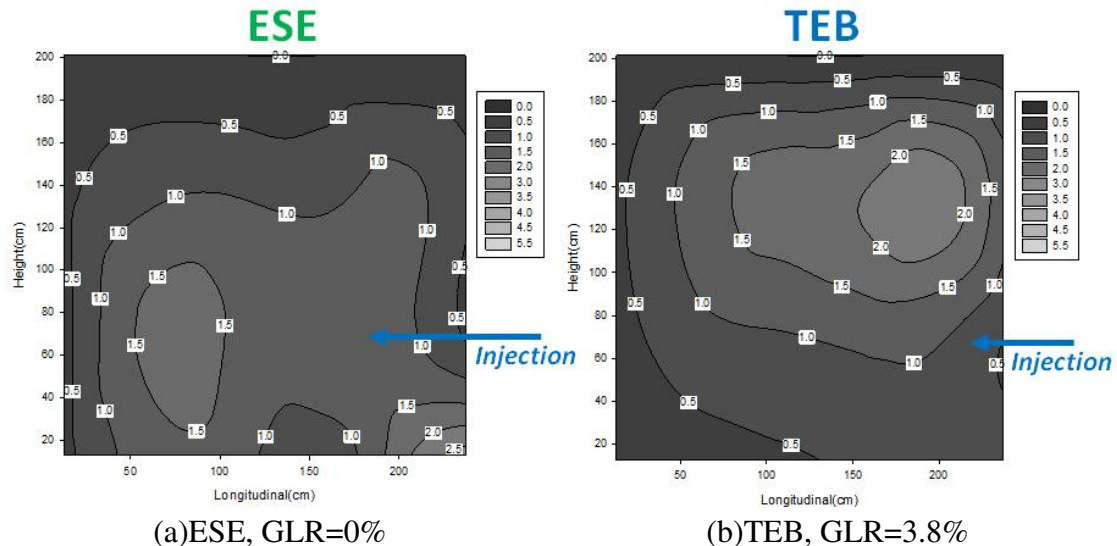


Figure 3.11 Comparison of two different GLR's of ESE and TEB which have similar injection quality

3.5 Conclusion

The performance of a commercial scale Fluid Coker nozzle in a large fluid bed was successfully investigated by a conductance method.

The distribution of injected liquid on fluidized particles was remarkably enhanced by adding a cylindrical draft tube downstream of the nozzle. Less liquid is trapped within wet liquid-solid agglomerates, which are detrimental to industrial reactor yields and operability. The liquid is also better distributed throughout the fluidized bed.

Implementing the ESE nozzle technology could help improve Fluid Cokers in two ways. First, liquid yields and reactor operability could be dramatically improved by operating the spray nozzles with the same atomization gas flow and adding ESE. Second, the atomization gas flowrate could be drastically reduced without any detrimental impact on coker yields and operability; this would reduce steam consumption, wastewater flows and allow for an increase in coker throughput.

3.6 Nomenclature

f	Free moisture
FCC	Fluid catalytic cracking
G/L	Gas-to-liquid mass ratio (wt%)
GLR	Gas-to-liquid mass ratio (wt%)
L	Width of the bed
L/S	Bed liquid-to-solid mass ratio (wt%)
N_x	Maximum of the length of the bed
N_y	Maximum of the height of the bed
R	Electrical resistance (Ω)
t	Time (s)
V_1	Voltage measured across function generator (V)
V_2	Voltage measured across resistor (V)
x	Length of the bed
y	Height of the bed

Greek Symbols

Π	Electrical conductance of fluidized bed (μS)
τ	Weight percentage ratio of free moisture over total injected moisture

3.7 References

- (1) Leach, A.; Chaplin, G.; Briens, C.; Berruti, F. Comparison of the performance of liquid–gas injection nozzles in a gas–solid fluidized bed. *Chemical Engineering and Processing: Process Intensification* **2009**, *48*, 780-788.
- (2) Portoghese, F.; House, P.; Berruti, F.; Briens, C.; Adamiak, K.; Chan, E. Electric conductance method to study the contact of injected liquid with fluidized particles. *AIChE J.* **2008**, *54*, 1770-1781.
- (3) House, P. K.; Saberian, M.; Briens, C. L.; Berruti, F.; Chan, E. Injection of a Liquid Spray into a Fluidized Bed: Particle–Liquid Mixing and Impact on Fluid Coker Yields. *Ind Eng Chem Res* **2004**, *43*, 5663-5669.
- (4) House P.; Berruti F.; Gray M.; Chan E.; Briens C.; Prediction of Propensity to Fouling in FluidCokers. AIChE National Meeting, San Francisco; November 12–17, **2006**.
- (5) Gray M.; Upgrading of petroleum residues and heavy oils. New York: Marcel Dekker, Inc; **1994**.
- (6) McMillan, J; Zhou, D; Saberian, M; Briens, C; Berruti, F. Measurement techniques to characterize the contact between injected liquid and circulating solids in a downer mixing chamber. *Powder Technology* **2006**, *161*, 175 – 184.
- (7) Mirgain, C.; Briens, C.L.; Del Pozo, M.; Loutaty, R.; Bergougnou, M.A. A new technique for the evaluation of a circulating fluidized bed mixing chamber with a central solids jet. *Powder Technology* **1998**, *96*, 202-210.
- (8) Zirgachianzadeh, M.; Soleimani, M.; Briens, C.; Berruti, F. Electric conductance method for the assessment of liquid-gas injection into a large gas-solid fluidized bed. *Measurement* **2012**, submission in progress
- (9) Portoghese, F.; Ferrante, L.; Berruti, F.; Briens, C.; Chan, E. Effect of injection-nozzle operating parameters on the interaction between a gas–liquid jet and a gas–solid fluidized bed. *Powder Technol* **2008**, *184*, 1-10.
- (10) Hulet, C.; Briens, C.; Berruti, F.; Chan, E.; Ariyapadi, S. Entrainment and Stability of a Horizontal Gas-Liquid jet in a Fluidized Bed. *Int. J. Chem. React. Eng.* **2003**, *1* (A60), 1127.
- (11) McMillan, J.; Zhou, D.; Ariyapadi, S.; Briens, C.; Berruti, F.; Chan, E. Characterization of the contact between liquid spray droplets and particles in a fluidized bed, *Ind. Eng. Chem. Res.* *44* **2005** 4931– 4939.

- (12) Ariyapadi S.; Holdsworth D.; Norley C.; Berruti F.; Briens C.; Digital X-ray imaging technique to study the horizontal injection of gas-liquid jets into fluidized beds. *Int J Chem React Eng.* **2003**;1:A56.
- (13) Ariyapadi, S.; McMillan, J.; Zhou, D.; Berruti, F.; Briens, C.; Chan, E. Modeling the mixing of a gas-liquid spray jet injected in a gas-solid fluidized bed: the effect of the draft tube, *Chem. Eng. Sci.* 60 (**2005**) 5738–5750.
- (14) Watano, S.; Sato, Y.; Miyanami, K. Application of fuzzy logic to moisture control in fluidized bed granulation, *Journal of Chemical Engineering of Japan* 28 (3) **1995** 282–287.
- (15) McCracken, T.; Bennett, A.; Jonasson, K.; Kirpalani, D.; Tafreshi, Z.; Base, T.; Emberley, D.; Kennett, R.; Bulbuc, D.; Chan, E. Nozzle for Atomizing Liquid in Two Phase Flow. U.S. Patent 0001062 A1, **2005**.
- (16) Base, T.; Chan, E.; Kennett, R.; Emberly, D. Nozzle for Atomizing Liquid in Two Phase Flow. U.S. Patent 6003789, **1999**.
- (17) Leach, A.; Portoghese, F.; Briens, C.; Berruti, F. A new and rapid method for the evaluation of the liquid-solid contact resulting from liquid injection into a fluidized bed. *Powder Technol* **2008**, 184, 44-51.
- (18) Weber, S.; Briens, C.; Berruti, F.; Chan, E.; Gray, M. Agglomerate stability in fluidized beds of glass beads and silica sand. *Powder Technol* **2006**, 165, 115-127.

Chapter 4: In-situ characterization of bed fluidity in a large gas-solid fluidized bed via electric conductance method

4.1 Introduction

Monitoring the fluidization quality represents an operating challenge for many processes in which a liquid is sprayed into a gas-fluidized bed, such as Fluid Coking, fluid catalytic cracking, gas-phase polymerization, agglomeration and drying. Although the presence of liquid will generally have an adverse effect on fluidization, as it might increase the cohesivity of particles and defluidize a part or the entire bed, there are often strong incentives in operating with high liquid loadings [1]. In Fluid Cokers, the heavy feedstock is sprayed onto hot coke particles and undergoes thermal cracking that yields lighter hydrocarbons and solid coke. The coke particles are continuously recirculated between the coker and a burner where some of the coke is combusted to reheat the particles. Excess coke is continuously removed from the system.

Operating data from the Syncrude fluid cokers have shown that reducing the Fluid Coker temperature provides two major benefits. Yields of valuable liquids are increased and sulphur oxide emissions are reduced by lowering the burner temperature, as sulphur is concentrated in the more refractory coke fractions that will no longer be combusted. There are, however, two major drawbacks to lower coker temperatures. First, fouling of stripper sheds increases. Second, lower temperatures reduce the reaction rate and thus unconverted feed may remain on the coke surface. This could lead to local zones of poor mixing and/or local defluidization, so called “boggling”, with detrimental effects on reactor performance and stability. The objective of this work is to apply and compare reliable methods to detect bogging under conditions relevant to fluid coking in large scale [2].

Various methods have been applied in the literature to detect the quality of fluidization. The apparent viscosity and fluidization quality of a fluidized bed are related [3]. Several investigators have measured the apparent viscosity of a fluidized bed with a paddle, rotating spheres, falling ball and Couette-type viscometers [3]. The results vary widely, and it is difficult to estimate apparent viscosities of such fluidized systems where

the peripheral velocities of immersed objects are of the same magnitude as particle velocities in the undisturbed bed [4, 5].

Several authors developed methods to detect defluidized zones between adjacent gas jets in the grid zone of a fluidized bed. Yutani et al. [6] used autocorrelation of local capacitance measurements. Industrial application of this method would be difficult as the capacitance probes require large electric potentials and may be too fragile for some processes.

Moreover, heat transfer measurements can also be used for the detection of defluidized zones. Ropchan [7] measured local heat transfer coefficients using a self-heated thermistor and found that defluidized zones could be detected from the fluctuations of the heat transfer coefficient. Marzocchella and Salatino [8] confirmed these results. Karamavruc_ and Clark [9] found that the Hurst exponent of temperature fluctuations could detect defluidized zones around a horizontal heat transfer tube. Heat transfer measurements however are not suitable for the detection of other kinds of defluidized zones in beds of polymer particles: thermistors and other heat transfer probes create hot spots which may result in sintering thereby promoting the formation of defluidized zones.

Defluidized zones were also reliably and rapidly detected by triboelectric currents generated at electrodes in the distributor zone of gas–solid fluidized beds [10]. Triboelectric currents are generated by the potential difference developed by the charging of particles by friction between two materials [11]. Accurate detection of defluidized zones required signal processing with the V-statistic, a criterion that was developed to identify cycles [12].

In addition, Tsujimoto et al. [13] tested a new non-intrusive measuring technique by applying an acoustic emission sensor to monitor the onset of unstable fluidization caused by the increase in moisture content in a fluidized bed granulator that leads to defluidization [5].

McDougall et al. [5] also developed reliable laboratory methods to quantify the eventual degradation of the bed fluidity and/or formation of agglomerates that resulted from the injection of a liquid in a fluidized bed. There is a strong need, however, for

methods that are quicker and that could be used in industrial reactors. They also need to use data that can be easily and reliably collected without perturbing reactor operation [1].

Several other experimental methods have been tested to estimate the bed fluidity. For instance, pressure measurements are often used to characterise fluidized bed hydrodynamics [14], and are also a good choice for industrial monitoring purposes, since they are easy to perform, inexpensive and reliable [15]. The quality of fluidization is related to the excess gas velocity. Since the fluidization quality affects the gas bubble properties, which in turn cause the pressure fluctuations, the pressure fluctuations are affected by the fluidization quality. The magnitude of pressure fluctuations can be readily evaluated using pressure transducers. Calculation of the variance of the differential pressure fluctuations can be carried out rapidly to give a measure of the fluidization quality [16]. In addition, the analysis of wall pressure fluctuations has been used for decades for the identification of the flow regimes in bubble columns, in order to determine the transition points and also to extract regime features [17].

Furthermore, pressure measurements can be easily and reliably obtained in high-temperature industrial reactors. Several investigators analyzed pressure signal fluctuations to characterize the fluidization quality of fluidized beds [2]. Tardos et al. [18] and Strusch et al. [19] used the time-averaged bed pressure drop to investigate destabilization and defluidization of fluidized beds due to agglomeration. However, this method cannot provide early warning of poor bed fluidity. Van Ommen et al. [15] and Schouten and Van den Bleek [20] detected changes in particle size distribution from chaos analysis of the bed pressure drop fluctuations. Van Ommen et al. [21] presented an enhanced attractor comparison method based on pressure fluctuation measurements for an early warning of agglomeration in fluidized beds which they validated using a 0.1m diameter fluidized bed. Van der Schaaf et al. [22] evaluated origin, propagation and attenuation of pressure waves in a gas-liquid fluidized bed using the time series analysis method. Van der Schaaf et al. [22] used the coherence between time series of pressure fluctuations measured simultaneously in a fluidized bed along the column height to determine the gas bubble size. Guo et al. [23] investigated dynamics of pressure fluctuation in a bubbling fluidized bed at high temperature using power spectral density function. Many of these methods were examined by Briens et al. [2] and found to provide

suitable distinction at the extreme conditions but did not provide early detection of the moderate but significant degradation of fluidization quality that occurs bogging conditions are approached. Briens et al. [2] found that moderate degradation in bed fluidity in a 1 m diameter pilot fluid coker could be detected from bed dynamic pressure fluctuations, using a new tool called W statistic.

Another approach, for laboratory measurements, is to conduct image analysis, and the simplest way to characterize fluidization quality is to take photos or videos through the transparent wall of a fluidized bed column. Although observations in the vicinity of the wall cannot always be representative of the gas–solid flow in the interior of the bed, investigations of this kind can be very helpful for an understanding of wall-related processes. The particle image velocimetry [24-26] which is based on a double-or multiple-exposure photography allows the reconstruction of the track of specially marked tracer particles. For example, in the multicolor stroboscopic photography used by Zheng et al. [25] successive red, blue and yellow images of white tracer particles in a fluidized bed of black particles provide particle velocities and directions of motion in the region adjacent to the wall [27].

Zirgachianzadeh et al. [28] showed that the distribution of water on fluidized particles can be characterized from the local bed conductivity. They performed reliable measurements of the bed conductivity with wall electrodes in a large fluidized bed.

The general objective of the study presented in this paper was, therefore, to apply the bed conductivity method to detect the localized bed defluidization in large gas-solid fluidized bed and to evaluate other non-invasive methods.

4.2 Apparatus

The fluidized bed used in the present study is the same as the one used in the previous study, [28], as it shown in Figure 4.1 andFigure 4.2. Water injections were atomized with nitrogen into the bed using a commercial-scale nozzle with the size and configuration as that of a fluid coker.

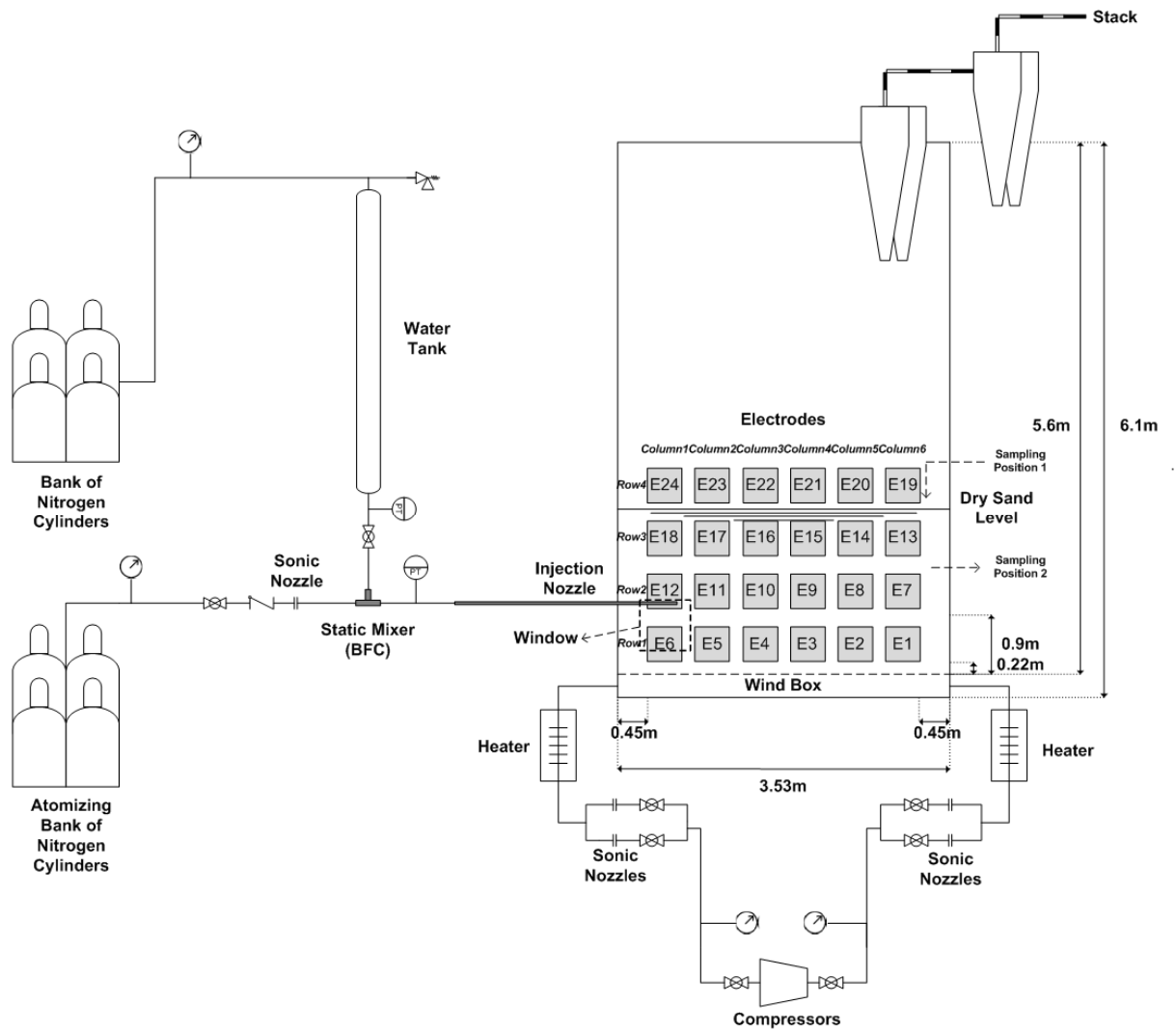


Figure 4.1 Schematic diagram of the experimental set-up



Figure 4.2 Experimental apparatus picture

The fluidized bed column had a trapezoidal cross-section of $3.5\text{m} \times 1.2\text{m} \times 0.2\text{m}$, and a height of 6.1 m to simulate one injection course of a fluid coker reactor (chosen based on previous jet expansion angle studies [29]), Figure 4.3.

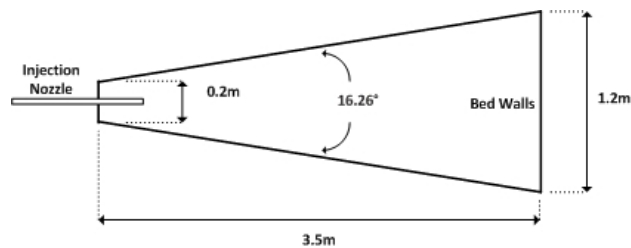


Figure 4.3 Top view of the bed

The large nozzle assembly was inserted 0.7m into the bed about 0.9 m above the distributor grid, at the narrow end of the bed. The atomization gas was pre-mixed with pressurized water upstream of the nozzle conduit, in a bilateral flow conditioner (BFC) [30]. The nozzle used in the tests used a geometry patented for commercial Fluid Cokers [31], Figure 4.4.



Figure 4.4 TEB Nozzle Scheme

The fluidized solid particles were silica sand particles with the same characteristics as the ones used by previous study [28]. The total mass of solids in the bed was about 7300 kg and the temperature was 22 °C.

A camera was set up in front of the window in the narrow side of the bed (Figure 4.5). Its signal was processed with image processing software.

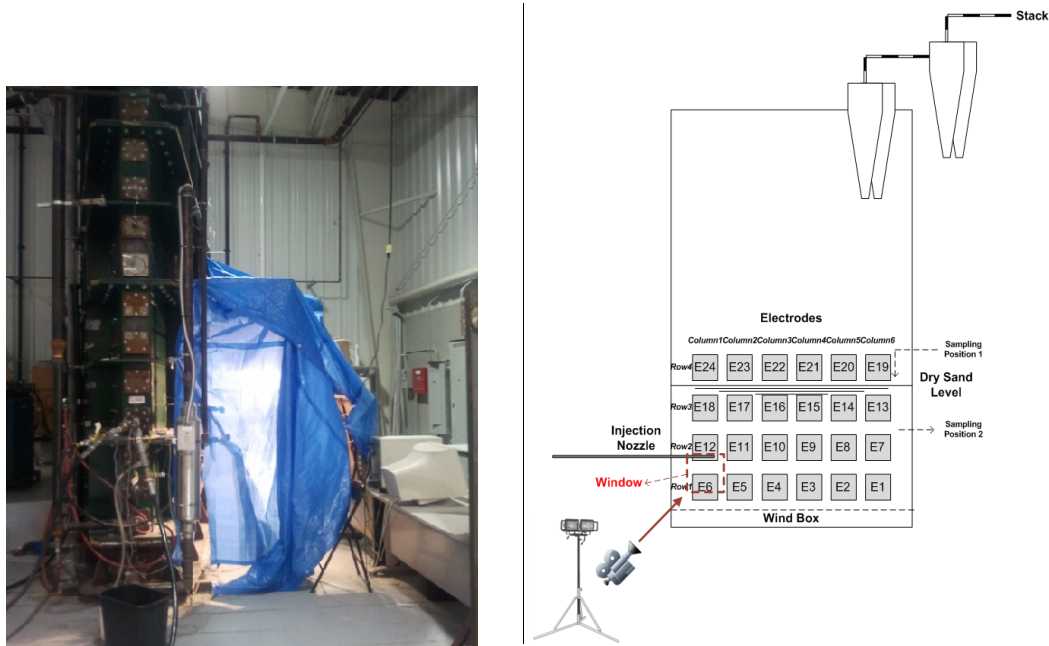


Figure 4.5 Camera set up in front of the window

Five thermometers as well as three J-type thermocouples positioned at different locations along the width and the length of the bed, and one another thermocouple in the freeboard helped ensure that the bed temperature was 22 °C at the start of each injection (Figure 4.6). Each one of the thermocouples penetrated 2 cm into the equipment to avoid significant stem losses.

A differential pressure transducer as well as a flush diaphragm pressure transducer measured the pressure fluctuations in the narrow side of the bed (Figure 4.6). The distance between the two sampling points of the differential pressure transducer was 35 cm.

Twenty-four 0.245×0.245 m (10×10 inch) electrodes were installed along the length of the bed to measure the local bed conductance during the experiments. Since bogging tended to occur primarily in the narrow side of the bed, Electrode 12, which was also located just above the window, was used for the conductance measurements (Figure

4.1). The other sensors were also installed in this section (Figure 4.6). A linoleum sheet electrically insulated the electrodes from the steel bed walls, which were electrically grounded. Schematic diagrams of the electrodes and sensors are shown in Figure 4.1 and Figure 2.6.

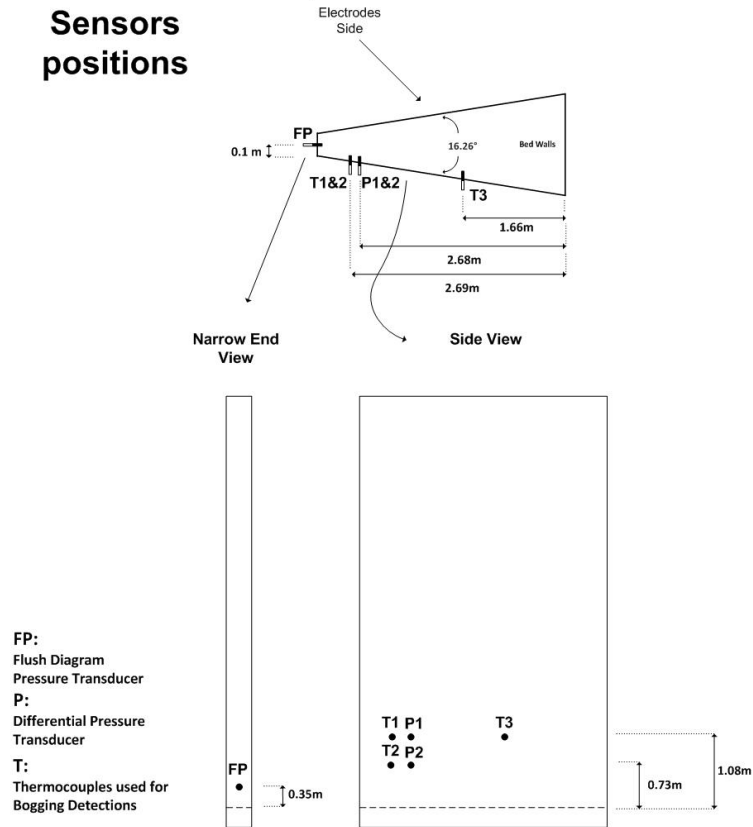


Figure 4.6 Schematic diagram of sensors configuration

The electrical set-up was exactly the same as the one used by Zirgachianzadeh et al.[28].

4.3 Experimental Procedure

A previous study [32] showed that the injected liquid normally ended up as either free moisture, distributed in a thin layer around individual bed particles, or as moisture trapped within liquid-solid agglomerates. Testing showed that the liquid trapped within agglomerates had a negligible impact on the bed conductance, which depends primarily

on the bed free moisture. Calibration experiments were used to determine the relationship between the local bed conductance and its free moisture [28].

The experimental procedure for bogging detection runs was as follows:

(1) To promote bogging in side one, only side one of the bed (see Figure 4.7) was fluidized before starting the injection for about 3 minutes with a fluidization air velocity of 0.15 m/s.

(2) A mass of water, which ranged from 2.5 to 17 kg, was then sprayed into the bed through the injection nozzle. In most experiments, the atomization gas to liquid flowrate mass ratio (GLR) was held constant at 4.2 %. In selected experiments, the mass of injected water was held constant at 5.4 kg with the GLR ranging from 0 to 5%.

(3) Once the injection was completed, side 1 of the bed was fluidized at 0.15 m/s for further 20 minutes (see Figure 4.7).

(4) The fluidization air was then set to 0.15 m/s through both sides of the bed. A high pressure gas jet on side one was used to help disrupt the bogged area of the bed and dry the bed. The drying end time was verified with the thermocouples.

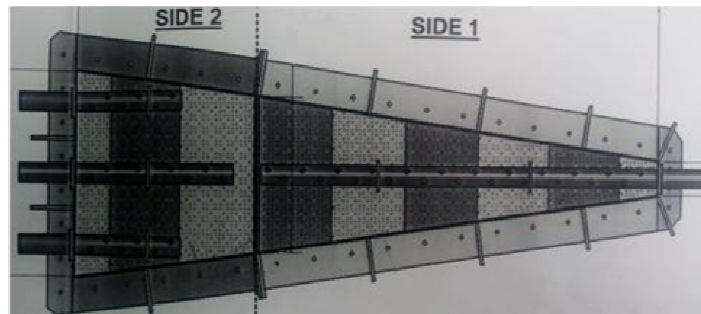


Figure 4.7 Wind box configuration

Measurements were performed with the conductance and other sensors during all the experiments. However, measurements during step (3) were the most important for the bogging detection.

Additional experiments were conducted to determine the local free moisture in the electrode 12 region. These experiments used steps (1), (2) and (3) as above, but the bed was defluidized after step (3) and the local conductance of the fluidized bed was used to determine the local free moisture, using the calibration curve for Electrode 12 from the previous study, [28] (Figure 4.8).

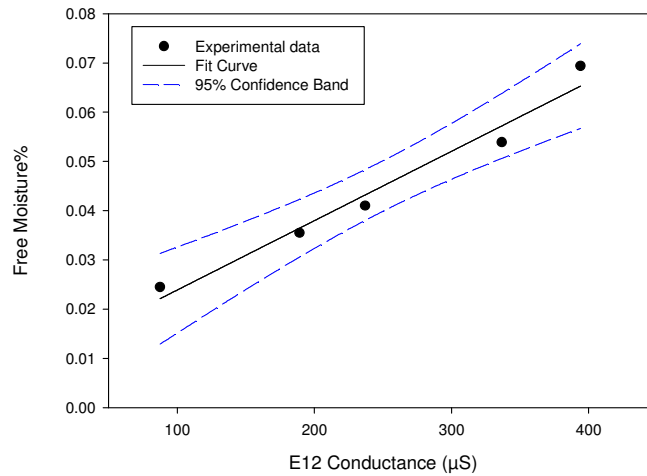


Figure 4.8 Calibration Curve for the defluidized bed

4.4 Results

4.4.1 Effect of Free Moisture on Bogging

All the experiments in this section were conducted with an atomization GLR of 4.2%. The local free moisture of the bed was varied by changing the mass of injected water.

Local bogging could be observed through a window on the bed wall. The left side of Figure 4.9 shows an image of the normal fluidization of the bed in which bubbles are going through easily whereas in the right side, under bogging conditions, air flowed under what appeared to be channeling conditions that are akin to what is observed with Geldart's group C particles. Accordingly, video imaging techniques were applied to the videos which were acquired through the window. Image analysis was performed on the video frames using Matlab.

An image analysis index was developed to identify bogging conditions from the videos. Figure 4.10 shows that local bogging can be clearly identified from the image analysis index. There is a rather short transition period. First the video frames obtained from the camera were converted to grey and then binary images of black and white pixels, with the black pixels corresponding to the bubbles. Afterwards, the Image

Analysis Index was obtained by summing up the changing black pixels; a high index corresponding to more bubbles, i.e. no bogging.



Figure 4.9 Left: bubbles going through the bed, Right: air being stuck in the sands

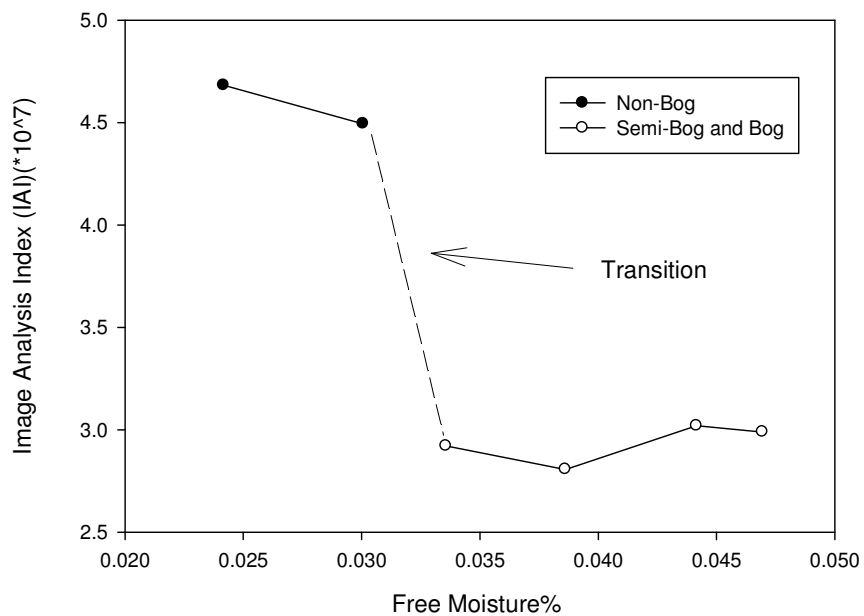


Figure 4.10 Image Processing results

Figure 4.11 shows that there was a good reproducibility of the conductance measurements. Because the GLR was only 2.24% to avoid any bogging, liquid-solid agglomerates were formed. All the injections started 126 s after the start of the signal acquisition, and were performed over a span of 11 s; it only took 5 s for the liquid to register on the conductance electrode 12.

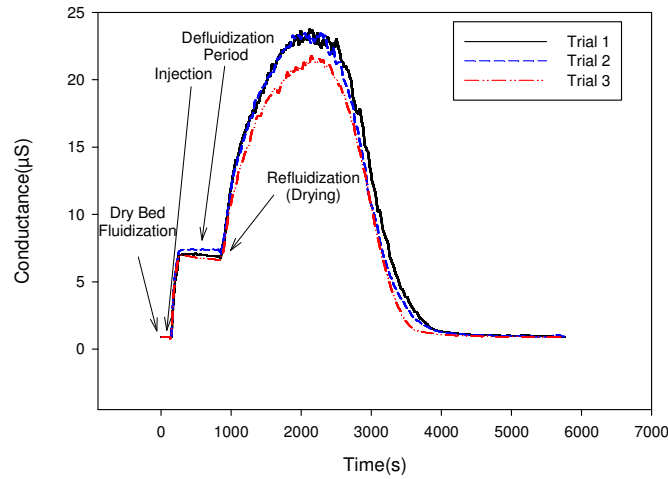


Figure 4.11 Conductance signal variation with time after the injections of GLR=2.24%. All the injections started at 126 s. Electrode 12.

The conductance signal increases during the liquid injection, remains constant during the defluidization period, and then increases progressively upon re-fluidization until 2200 s, i.e. about 1355 s after the start of re-fluidization. It therefore took about twenty-two minutes for the liquid to spread enough to maximize the free moisture. Because of evaporation, the free moisture and the signal then decreased slowly until about 5000 s, the drying end point. Figure 4.11 shows that during re-fluidization, agglomerates are breaking up, generating additional free moisture, while free moisture disappears through evaporation; at first, the free moisture increases as the free moisture added through agglomerate breakup is greater than the free moisture disappearing through evaporation while, past the conductance peak, the effect of evaporation predominates [1, 32].

The section of the bed that is in front of electrode 12 (Figure 4.1), is prone to bog since it is close to the injection nozzle and also in the narrowest side of the bed where there is a high concentration of water [28]. This electrode has, therefore, been used for the study of local bogging.

Figure 4.12, shows the twelfth electrode conductance signal obtained from two different experiments with small ratios of injected liquid to dry bed solids (L/S). The signal behaviour is as in Figure 4.11. As expected, the bed conductance is higher when

the mass of injected liquid is higher and it is quite sensitive to this mass of injected liquid, demonstrating the sensitivity of the conductance measurements.

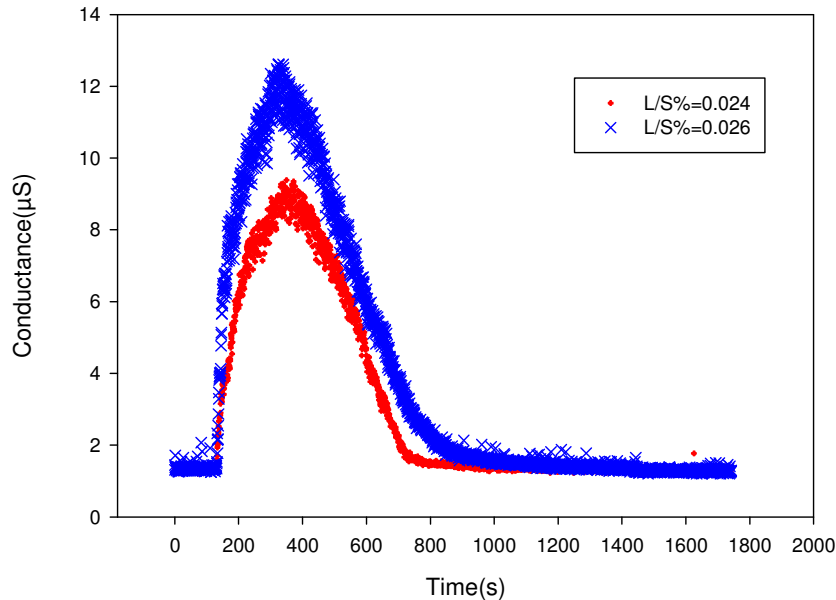


Figure 4.12 Electrode 12th signal when there is no local bogging

Figure 4.13 shows that when the mass of injected liquid is increased, a sudden change appears in the middle of the raise of the signal. This is similar to what is observed when cutting off the fluidization air, as shown in Figure 4.11. In the case of Figure 4.13, however, the fluidization air is still on and defluidization is caused by bogging.

Figure 4.14 shows, for comparison, the signals obtained from electrode 11 at injected liquid to solid ratios for which defluidization was observed with electrode 12. Electrode 11 shows that there was no defluidization. Electrode 11 is located just beside Electrode 12 but in the wider section of the bed. This shows that bogging is a local phenomenon and that can easily be detected by local conductance measurements.

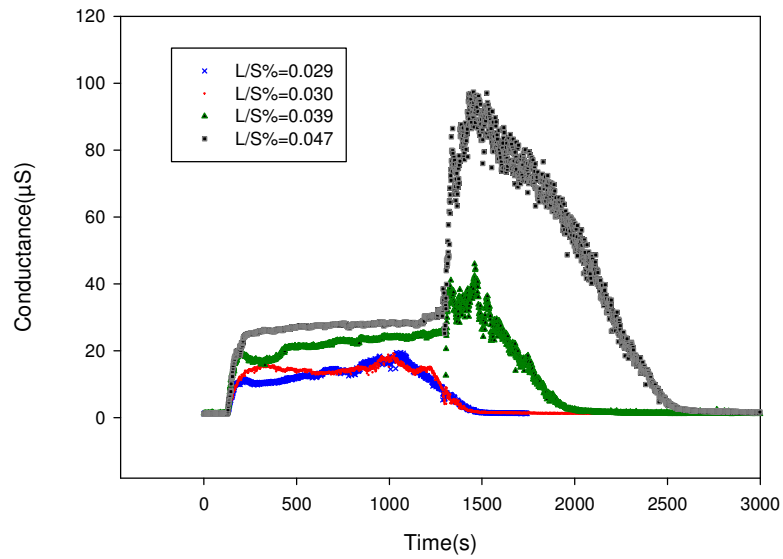


Figure 4.13 Electrode 12th signal with local bogging

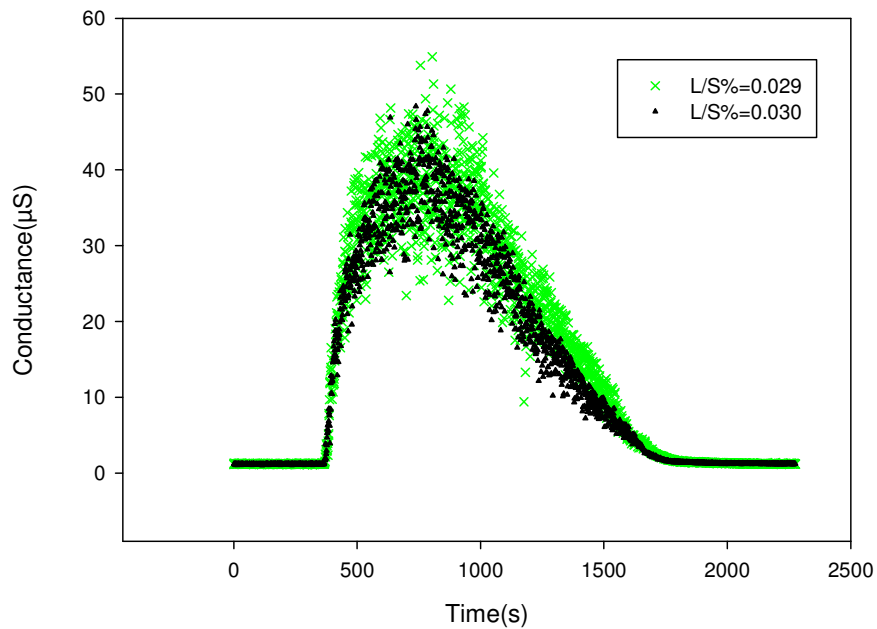


Figure 4.14 Electrode 11th signal when its facing area has been bogged for a while

Figure 4.15 shows that the coefficient variance of the conductance signal from electrode 12 can be used to detect localized bogging. Coefficient of variance is a normalized measure of dispersion of a probability distribution and is defined as the ratio of the standard deviation to the mean. This method agrees well with the image

analysis method (Figure 4.10), applied to the videos through a window in nearly the same location as electrode 12.

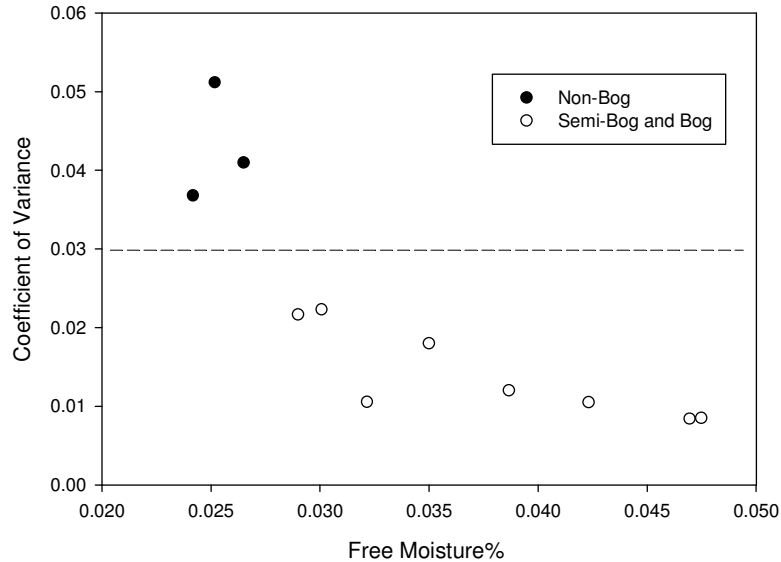


Figure 4.15 Coefficient of Variance of the twelfth electrode

Pressure fluctuations can also be used to detect bogging. A differential Pressure transducer was installed in front of electrode 12, on the opposite bed wall (Figure 4.1). Figure 4.16 and Figure 4.17 show that there was a dramatic change in the type of signal obtained from this transducer when going from normal fluidization to bogging. When there is no bogging, the amplitude of the pressure fluctuations is about the same as in the dry bed, before the liquid injection (Figure 4.16), while, when bogging occurs, the amplitude of the pressure fluctuations is constant at a reduced value (Figure 4.17). In addition, when there is no bogging, the distribution of the data after the injection is almost the same as before it (Figure 4.16) where as when bogging occurs the distribution is much reduced after the injection (Figure 4.17).

Figure 4.18 confirms that bogging can be detected from the coefficient of variance of the differential pressure fluctuations. Its results agree well with the results from image analysis (Figure 4.10) and the coefficient of variance of conductance fluctuations (Figure 4.15).

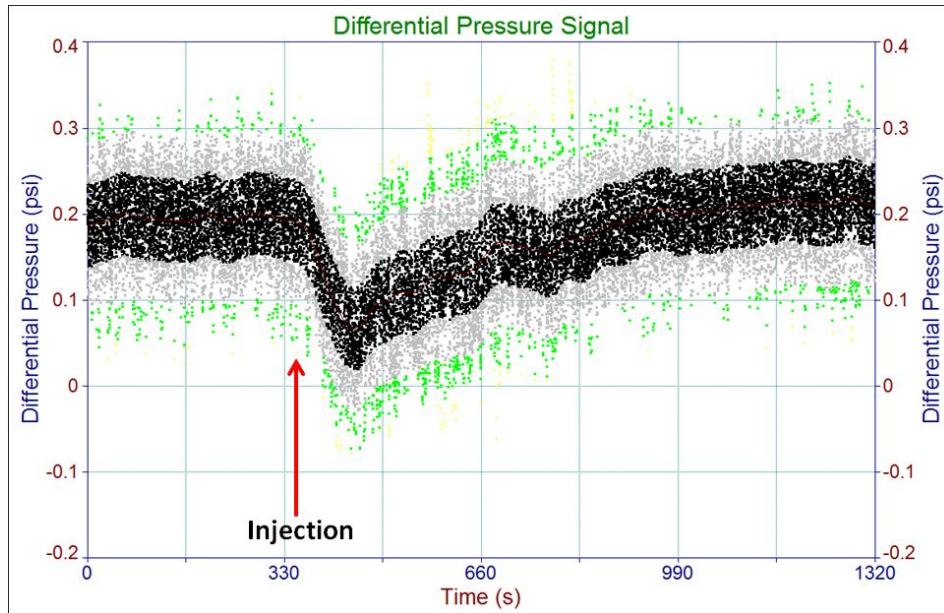


Figure 4.16 Differential Pressure Transducer signal when low liquid load is injected ($L/S = 0.024\%$), non-bogged conditions

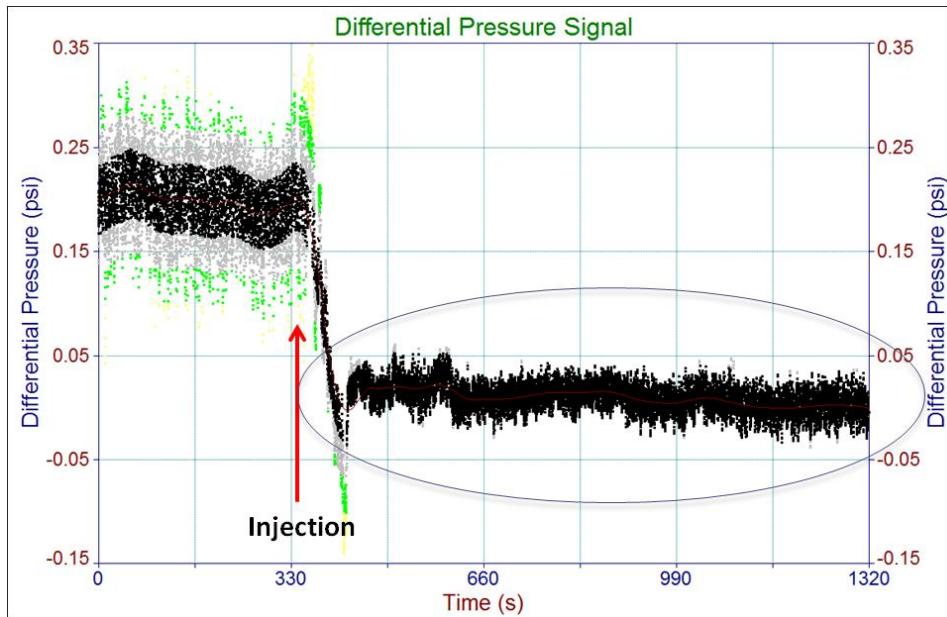


Figure 4.17 Differential Pressure Transducer signal when high liquid load is injected ($L/S = 0.047\%$), bogged conditions

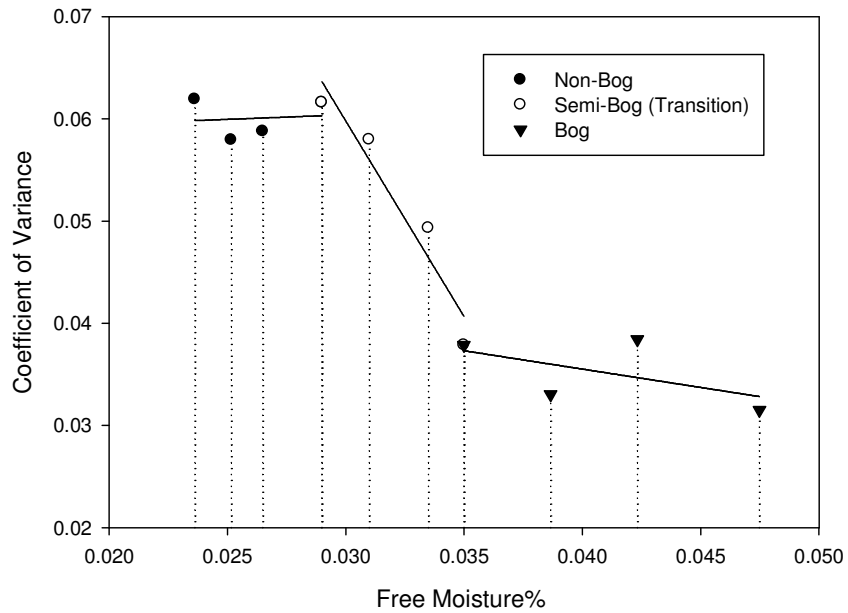


Figure 4.18 Coefficient of variance of the Differential Pressure Transducer signal

The coefficient variance of the local static pressure fluctuations measured by a flush diaphragm pressure transducer also agree well with the other methods, as shown by Figure 4.19. This type of pressure transducer can easily and reliably be used in industrial units, since it does not require filters or backflushing gas. Although its frequency response is not as good as the other transducer, this did not seem to affect its ability to detect bogging.

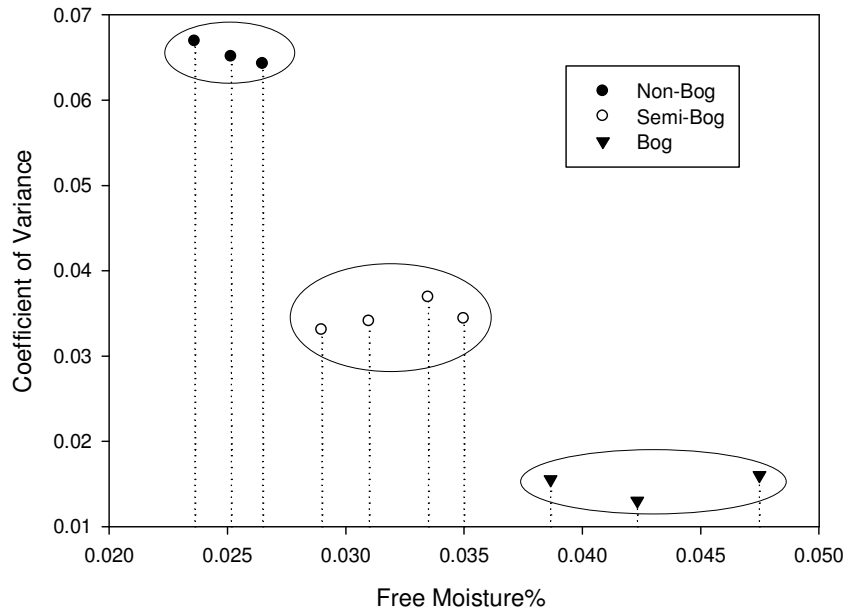


Figure 4.19 Coefficient of variance of the Flush Diagram Pressure Transducer signal

Figure 4.20 shows that bogging can be detected from the difference in temperature between the bogging and non-bogging regions of the bed as well, although it does seem to be able to differentiate between semi-bogged and fully bogged conditions. The temperature of the bogging zone was measured with T1 and T2, the average of them being called $T_{av.}$, and the temperature of the non-bogging zone was measured with T3 (Figure 4.6). In bed regions that are bogged, there is not as much drying and the temperature does not drop as much as in well-mixed regions, where there is intense evaporation of the free moisture.

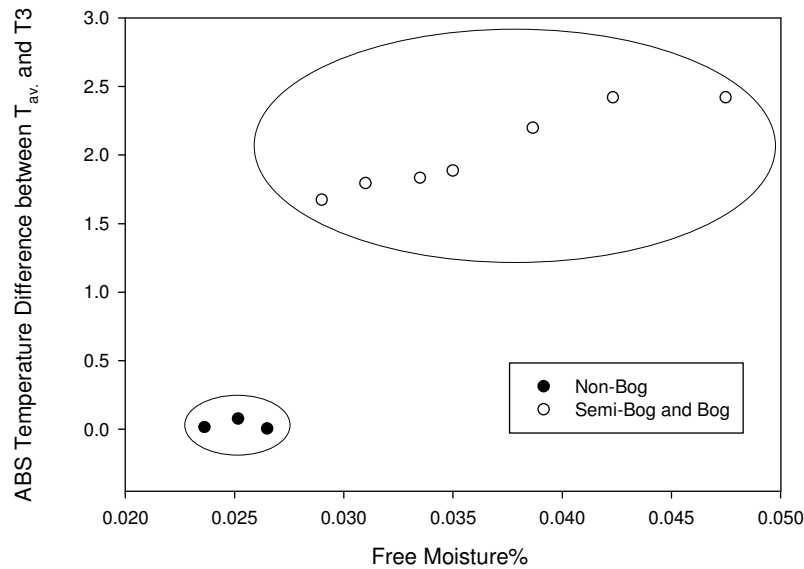


Figure 4.20 Absolute difference between thermocouples signals in bogging and non-bogging zones

4.4.2 Verification that Bogging Depends on Free Moisture

Another set of experiments was carried out to confirm that bogging was related to the free moisture and not the total moisture, which includes the water trapped in wet agglomerates. In these experiments, the total moisture was kept constant by injecting the same amount of water, but the free moisture was varied by adjusting the atomization GLR, which has been shown to have a strong effect on the free moisture [28].

Figure 4.21, Figure 4.22 and Figure 4.23 show clearly that although the total moisture was kept constant as 5.4 kg of water was injected all the time, the local bed fluidization moved from non-bogged to bogged conditions as the GLR was increased, raising the free moisture level. The transition from non-bogged to bogged conditions occurred when the free moisture increased beyond 0.032%.

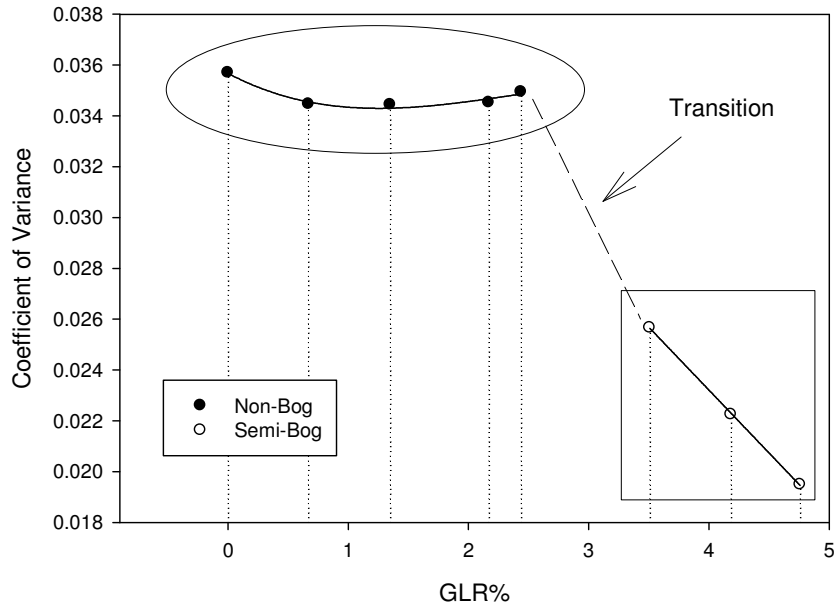


Figure 4.21 Coefficient of variance of electrode 12 for different GLR's

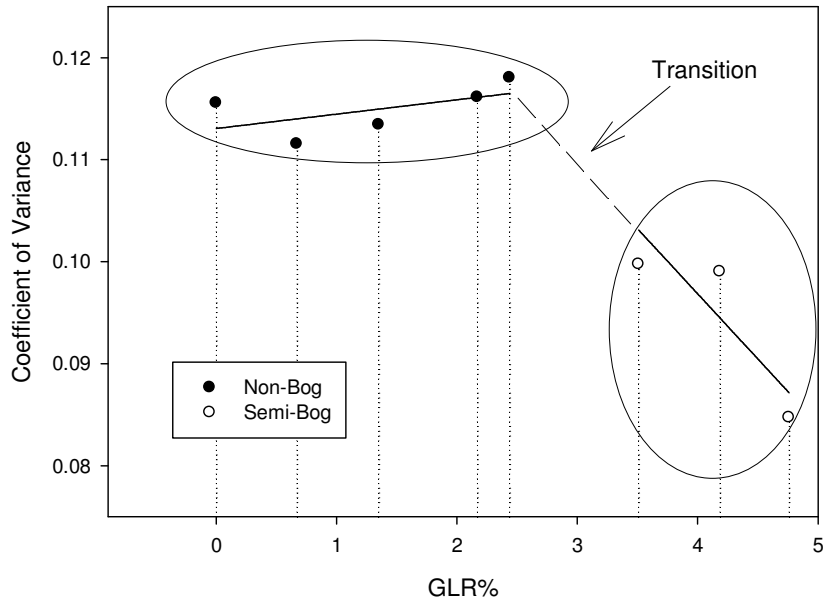


Figure 4.22 Coefficient of variance of the Differential Pressure Transducer for different GLR's

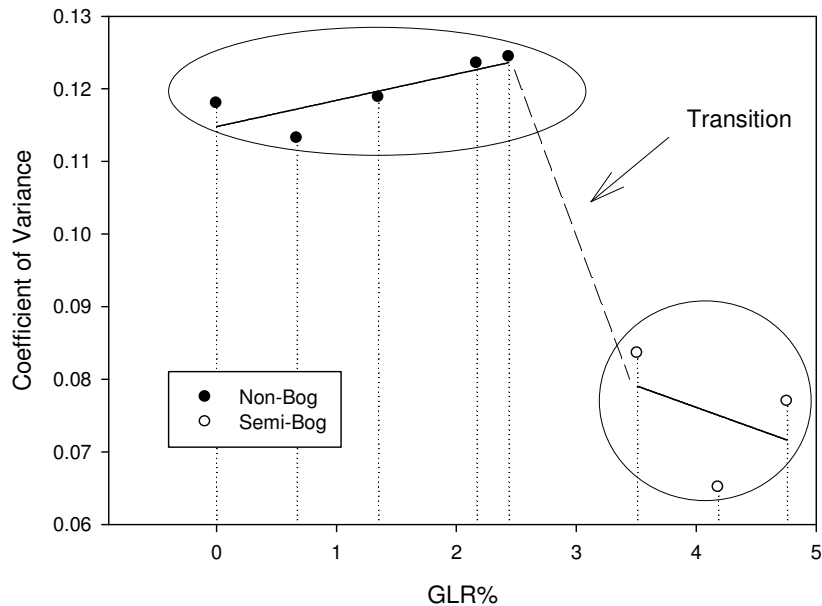


Figure 4.23 Coefficient of variance of the Flush Diagram Pressure Transducer for different GLR's

4.5 Conclusion

A novel method employing electrical conductance was successfully developed to detect local defluidization or “boggging” caused by liquid injection in a large scale pilot fluidized bed of about 7 tonnes of silica sand. Several other experimental methods, such as image processing, and the fluctuations of differential or static pressure measurements, were also successful.

When liquid is injected into a fluidized bed, a fraction forms liquid-solid agglomerates while the remainder forms free moisture, consisting of individual particles coated with a thin layer of liquid. The results indicated that conductance measurements could be used for detecting bogging phenomena online. Bogging is directly associated with the local free moisture rather than the total moisture level. In fact, there is a measurable critical, local free moisture value above which localized bogging occurs.

4.6 Nomenclature

FCC Fluid catalytic cracking

G/L	Gas-to-liquid mass ratio (wt%)
GLR	Gas-to-liquid mass ratio (wt%)
L	Width of the bed
L/S	Bed-averaged mass ratio of injected liquid to dry bed solids (wt%)
NPI	Nozzle performance index (—)
R	Electrical resistance (Ω)
t	Time (s)
V ₁	Voltage measured across function generator (V)
V ₂	Voltage measured across resistor (V)
V _{gs}	Superficial gas velocity (m/s)

Greek Symbols

Π	Electrical conductance of fluidized bed (μS)
-------	---

4.7 References

1. McDougall, S.; Saberian, M.; Briens, C.; Berruti, F.; Chan, E. Using dynamic pressure signals to assess the effects of liquid injection on fluidized bed properties, submitted to Chemical Engineering and Processing, **2004**.
2. Briens, C.; McDougall, S.; Chan, E.W. On-line detection of bed fluidity in a fluidized bed coker, Powder Technol. 138 (**2003**) 160–168.
3. Kai, T.; Murakami, M.; Yamasaki, K.I.; Takahashi, T. “Relationship between apparent bed viscosity and fluidization quality in a fluidized bed with fine particles”, J. Chem. Eng. Japan, Vol. 24, No. 4, 494-500 (**1991**)
4. Grace, J.R. “The viscosity of fluidized beds”, Can. J. Chem. Eng., Vol. 48, 30-33 (**1970**)
5. McDougall, S.; Saberian, M.; Briens, C.L.; Berruti, F.; Chan, E.W. Characterization of fluidization quality in fluidized beds of wet particles, Int. J. Chem. React. Eng. 2 (**2004**) A26.
6. Yutani, N.; Ho, T.C.; Fan, L.T.; Walawender, W.P.; Song, J.C. Statistical study of the grid zone behavior in a shallow gas—solid fluidized bed using a mini-capacitance probe Chem. Eng. Sci. 38 (**1983**) 575.
7. Ropchan W.T. Heat transfer and grid jets, PhD Thesis, Stanford University, (**1981**).

8. Marzochella A.; Salatino, P. National AIChE Meeting, (1995).
9. Karamavruc, A.I.; Clark, N.N.; Powder Technology 90 (1997) 235.
10. Briens, C.L. ; Briens, L.A. ; Barthel, E. ; Le Blévec, J.M. ; Tedoldi, A. ; Margaritis, A. Powder Technology 102 (1999) 95.
11. Moore (Ed.), A.D. Electrostatics and its Applications, Wiley, USA, 1974, p. 64.
E.E. Peters, Applying Chaos Analysis to Investment and Economics, Wiley, New York, 1994.
12. Peters, E.E. Applying Chaos Analysis to Investment and Economics, Wiley, New York, 1994.
13. Tsujimoto, H.; Yokoyama, T.; Huang, C.C.; Sekiguchi, I. Monitoring particle fluidization in a fluidized bed granulator with an acoustic emission sensor, Powder Technology, Vol. 113, 88-96 (2000)
14. Yates, J.G.; Simons, S.J.R. Int. J. Multiphase Flow 20 (1994) Suppl., pp. 297-330
15. Van Ommen, J. R.; Schouten J. C.; Coppens, M.-O.; van den Bleek, C. M. Monitoring Fluidization by Dynamic Pressure Analysis," Chem. Eng. Technol., 22, 773 _1999d.
16. Chong, Y. O.; O'dea, D. P.; White, E. T.; Lee, P. L.; Leung, L. S. Control of the Quality of Fluidization in a Tall Bed Using the Variance of Pressure Fluctuations Powder Technol., 53, 237-246 (1987)
17. Gourich B.; Vial C.; Essadki A.; Allam, F.; Soluami, M.; Ziyad M. Identification of Flow Regimes and Transition Points in a Bubble Column Through Analysis of Differential Pressure Signal- Influence of the Coalescence Behavior of the Liquid Phase, Chemical Engineering and Processing, 45, 214-223, 2006.
18. Tardos, G.; Mazzone, D.; Pfeffer, R. Destabilization of fluidized beds due to agglomeration - part II: Experimental verification, Canadian Journal of Chemical Engineering, 63(1985) 384-389
19. Strusch, J.; Riehle, C.; Mleczko, L. Development of a method for preparing particles for the investigations of defluidization phenomena in cold flow models, Bayer, Nuremberg, PARTEC 2001
20. Schouten, J.C.; Van den Bleek, C.M. Monitoring the quality of fluidization using the short term predictability of pressure fluctuations, AIChE J., 44(1998) 48-60
21. Van Ommen, J.R.; Coppens, M. O.; Van den Bleek, C. M.; Schouten, J. Early warning of agglomeration in fluidized beds by attractor comparison, AIChE J., 46 11(2000) 2183- 2197
22. Van der Schaaf, J.; Schouten, J.C.; Van den Bleek, C.M. Non-intrusive determination of bubble and slug length scales in fluidized beds by decomposition of the power spectral density of pressure time series, International Journal of Multiphase Flow, 28(2002) 865- 880
23. Guo, Q.; Yue, G.; Werther, J. Dynamic of pressure fluctuations in a bubbling fluidized bed at high temperature, Ind. Eng. Chem Res. 41(2002) 3482-3488
24. Chen, R.C.; Fan, L.S. Particle image velocimetry for characterizing the flow structure in three-dimensional gas-liquid-solid fluidized beds, Chem. Eng. Sci. 47 _1992. 3615-3622.
25. Zheng, Z.; Zhu, J.; Grace, J.R.; Lim, C.J.; Brereton, C.H.M. Particle motion in circulating and revolving fluidized beds via microcomputer- controlled colour-stroboscopic photography, in: O.E. Potter, D.J. Nicklin _Eds., Fluidization VII,

- Proc. 7th Int. Engineering Foundation Conf. Fluidization, Engineering Foundation, New York, **1992**, pp. 781–789.
26. Rix, S.J.L.; Glass, D.H.; Greated, C.A. Preliminary studies of elutriation from gas-fluidized beds using particle image velocimetry, *Chem. Eng. Sci.* 51 _1996. 3479–3489.
 27. Werther, J. Measurement techniques in fluidized beds, *Powder Technol.* 102 (**1999**) 15–36.
 28. Zirgachianzadeh, M.; Soleimani, M.; Briens, C.; Berruti, F. Electric conductance method for the assessment of liquid-gas injection into a large gas-solid fluidized bed. Measurement 2012, submission in progress.
 29. Ariyapadi S.; Holdsworth D.; Norley C.; Berruti F.; Briens C.; Digital X-ray imaging technique to study the horizontal injection of gas-liquid jets into fluidized beds. *Int J Chem React Eng.* **2003**;1:A56.
 30. McCracken, T.; Bennett, A.; Jonasson, K.; Kirpalani, D.; Tafreshi, Z.; Base, T.; Emberley, D.; Kennett, R.; Bulbuc, D.; Chan, E. Nozzle for Atomizing Liquid in Two Phase Flow. U.S. Patent 0001062 A1, **2005**.
 31. Base, T.; Chan, E.; Kennett, R.; Emberly, D. Nozzle for Atomizing Liquid in Two Phase Flow. U.S. Patent 6003789, **1999**.
 32. Portoghese, F.; Berruti, F.; Briens, C. Continuous on-line measurement of solid moisture content during fluidized bed drying using triboelectric probes. *Powder Technol* **2008**, 181, 169-177.

Chapter 5: Conclusions and Recommendations

5.1 Conclusions

1. A novel and reliable measurement technique using electrical conductance was successfully applied in a large fluidized bed to investigate the performance of an industrial scale Fluid Coker spray nozzle in terms of the quality of the distribution of the liquid feed on the bed particles.
2. It was found that operating at much higher atomization gas flow rates than what is used regularly is greatly beneficial. Not only is the liquid trapped in agglomerates reduced but the distribution of water over the whole bed volume is more uniform. This would result in a higher yield of valuable products in a Fluid Coker, as well as improved operability.
3. As using very high atomization gas flow rates would increase steam consumption in a Fluid Coker, another study was conducted to assess the effect of adding a cylindrical draft tube, called ESE, downstream of the industrial scale nozzle. ESE not only remarkably reduced the liquid trapped within wet agglomerates, but also greatly enhanced the distribution of injected liquid feed on fluidized particles over the whole bed volume. It also increased the penetration of the spray jet in the fluidized bed. Implementing the ESE nozzle technology could help improve Fluid Cokers in two ways. First, reactor operability and liquid yields could be improved by operating the spray nozzles with the same atomization gas flow and adding ESE. Second, the atomization gas flowrate could be drastically reduced without any detrimental impact on coker yields and operability; this would reduce steam consumption, wastewater flows and allow for an increase in coker throughput.
4. The conductance technique was also successfully implemented to detect local defluidization or “bogging” caused by liquid injection in the large scale pilot fluidized bed with about 7 tonnes of silica sand. Various other experimental methods, such as image processing, and the fluctuations of differential or static pressure measurements, were also successful in detecting local bogging. When liquid is injected into a fluidized bed, a fraction forms liquid-solid agglomerates

while the remainder forms free moisture, consisting of individual particles coated with a thin layer of liquid. It was found that conductance measurements could be used for the online detection of local bogging. The study also showed that bogging is directly associated with the local free moisture rather than the total moisture level. In fact, there is a measurable critical, local free moisture value above which localized bogging occurs.

5.2 Recommendations

1. The study on the operating conditions of the commercial scale nozzle suggested that although it is beneficial to use a nozzle at higher atomization flow rates than commonly used ones, the specific nozzle used had its own optimum performance range, with a highly non-linear relationship between nozzle performance and atomization gas flowrate. Future work should investigate whether other types of nozzles used in industry exhibit the same behaviour.
2. In the study on the effect of the draft tube on injection, only one distance between the draft tube and nozzle and only one draft tube configuration was used, extrapolating from studies with small scale nozzles. Future work should investigate the influence of changing this distance and also the configuration. The effect of draft tube on jet penetration should be investigated further.
3. One constraint for applying the draft tube in industry is fouling on the draft tube. Future work should investigate fouling phenomena for a draft tube used downstream of the nozzle.
4. The study on detection of bogging showed that the localized bogging phenomena could be detected by conductance technique and some other measurement techniques in a large scale fluidized bed. Future work should be on examining whether methods based on pressure measurements measure the local or global bogging. It should also verify the findings of this study for other fluidization velocities.

Curriculum Vitae

Name: MohammadAli Zirgachianzadeh

Post-secondary Education and Degrees: University of Shiraz
Shiraz, Iran
2003-2008 B.Sc.

Ecole Nationale Supérieure du Pétrole et des Moteurs (IFP School)
Île-de-France, France
2008-2010 M.Sc.

Honours and Awards: Western Engineering Scholarship
2010-2012

Related Work Experience Research Assistant
Institute for Chemicals and Fuels from Alternative Resources (ICFAR)
Western University
20010-2012

Teaching Assistant
Western University
2010-2011